

Spatiotemporal Organization of Simple-Cell Receptive Fields in the Cat's Striate Cortex. II. Linearity of Temporal and Spatial Summation

G. C. DEANGELIS, I. OHZAWA, AND R. D. FREEMAN

Groups in Bioengineering and Neurobiology, and School of Optometry, University of California,
Berkeley, California 94720

SUMMARY AND CONCLUSIONS

1. We have tested the hypothesis that simple cells in the cat's visual cortex perform a linear spatiotemporal filtering of the visual image. To conduct this study we note that a visual neuron behaves linearly if the responses to small, brief flashes of light are mathematically related, via the Fourier transform, to the responses elicited by sinusoidal grating stimuli.

2. We have evaluated the linearity of temporal and spatial summation for 118 simple cells recorded from the striate cortex (area 17) of adult cats and kittens at ages 4 and 8 wk postnatal. These neurons represent a subset of the population of cells for which we have described the postnatal development of spatiotemporal receptive-field structure in the preceding paper. Spatiotemporal receptive-field profiles are constructed, with the use of a reverse correlation technique, from the responses to random sequences of small bar stimuli that are brighter or darker than the background. Fourier analysis of spatiotemporal receptive-field profiles yields linear predictions of the cells' spatial and temporal frequency tuning. These predicted responses are compared with spatial and temporal frequency tuning curves measured by the use of drifting, sinusoidal-luminance grating stimuli.

3. For most simple cells, there is good agreement between spatial and temporal frequency tuning curves predicted from the receptive-field profile and those measured by the use of sinusoidal gratings. These results suggest that both spatial and temporal summation within simple cells are approximately linear. There is a tendency for predicted tuning curves to be slightly broader than measured tuning curves, a finding that is consistent with the effects of a threshold nonlinearity at the output of these neurons. In some cases, however, predicted tuning curves deviate from measured responses only at low spatial and temporal frequencies. This cannot be explained by a simple threshold nonlinearity.

4. If linearity is assumed, it should be possible to predict the direction selectivity of simple cells from the structure of their spatiotemporal receptive-field profiles. For virtually all cells, linear predictions correctly determine the preferred direction of motion of a visual stimulus. However, the strength of the directional bias is typically underestimated by a factor of about two on the basis of linear predictions. Consideration of the expansive exponential nonlinearity revealed in the contrast-response function permits a reconciliation of the discrepancy between measured and predicted direction selectivity indexes.

5. Overall, these findings show that spatiotemporal receptive-field profiles obtained with the use of reverse correlation may be used to predict a variety of response properties for simple cells. These results are generally consistent with recent theoretical work in which simple cells are modeled as the combination of a linear spatiotemporal filter, an exponent nonlinearity, and a contrast normalization mechanism.

INTRODUCTION

Early explorations of neuronal response properties in the striate cortex (area 17) have led to two different views of the function of simple cells. Hubel and Wiesel (1959, 1962) first discovered that simple cells respond optimally to bars and edges of light having a particular orientation in space. Hubel and Wiesel also reported that the optimal bar and edge stimuli for these neurons could be predicted on the basis of a qualitative mapping of their receptive fields. Additional studies of cortical cells using bars and edges of light (e.g., Bishop et al. 1971) have led some researchers to model simple cells as bar and edge detectors (e.g., Lindsay and Norman 1972). In an alternative approach, Campbell et al. (1969) and Cooper and Robson (1968) first measured the response properties of simple cells in the frequency domain, with the use of sinusoidal grating stimuli of variable spatial frequency. On the basis of these spatial frequency tuning measurements, it has been suggested (e.g., Albrecht et al. 1980; DeValois et al. 1982; Maffei and Fiorentini 1973) that simple cells act as spatial frequency analyzers.

These two seemingly contradictory views of simple-cell function have prompted an investigation (see Albrecht et al. 1980) as to whether the responses of cortical cells are more selective for bar or grating stimuli. The results of this study suggest that the responses of simple cells to both types of stimuli may be explained on the basis of linear spatial summation. For a linear spatial filter, the responses to bars and gratings can be related analytically through the Fourier transform. Moreover, it has been pointed out (Daugman 1985; Marcelja 1980) that a particular class of linear spatial filter, the Gabor filter (Gabor 1946), has maximal joint resolution in both the space and spatial frequency domains. Several investigators (Andrews and Pollen 1979; DeValois et al. 1978; Glezer et al. 1980, 1982; Kulikowski and Bishop 1981a; Maffei et al. 1979; Movshon et al. 1978; Tadmor and Tolhurst 1989; Webster and DeValois 1985) have evaluated whether spatial summation in simple cells is a linear process, by comparing the receptive-field profile measured by the use of bars (i.e., the "line-weighting function") with linear predictions on the basis of spatial frequency tuning curves measured with gratings. Some researchers (e.g., Glezer et al. 1982; Kulikowski and Bishop 1981a) have also conducted this evaluation in the frequency domain by comparing measured spatial frequency tuning curves with linear predictions obtained through Fourier analysis of the receptive-field profile. The general consensus of these stud-

ies, with the use of either method, is that simple cells sum their inputs over space in an approximately linear fashion. Studies using two-dimensional patterns (checkerboards and plaids) have also yielded results that support the notion that simple cells behave as linear spatial filters (DeValois et al. 1979). Moreover, it has been shown that Gabor functions provide a good fit to either the one-dimensional (Baker and Cynader 1986; DeAngelis et al. 1991a; Field and Tolhurst 1986; Marcelja 1980) or two-dimensional (Jones and Palmer 1987b; Webster and DeValois 1985) spatial receptive-field profiles of simple cells.

These findings have been taken as supporting evidence for models of visual cortical function in which simple cells perform a linear spatial filtering of the visual input (e.g., Geisler and Hamilton 1986; Kulikowski and Bishop 1981b; Sakitt and Barlow 1982; Watson 1983, 1987; Robson 1975, 1983). The advantage of a linear spatial filter is that its response to any spatial pattern can be predicted knowing only its impulse response (i.e., its receptive-field profile). However, the input to a visual neuron is not just a static spatial pattern, but a *spatiotemporal* pattern of luminance variation. In the companion paper (DeAngelis et al. 1993), we have described the spatiotemporal receptive-field structure of simple cells in the cat's striate cortex. For us to correctly predict the response of a simple cell to any time-varying visual pattern, based on the spatiotemporal receptive-field profile, the cell must exhibit not only linear spatial summation but also linear *temporal summation*.

Relatively little attention has been paid to the linearity of temporal summation in simple cells. Tolhurst et al. (1980) have compared temporal frequency tuning curves measured by the use of counterphase modulated gratings with predicted tuning curves obtained via Fourier analysis of the response to the onset of a flashed grating stimulus. They conclude that temporal summation in simple cells is grossly nonlinear because predicted temporal frequency tuning curves do not resemble measured tuning curves. This finding has been confirmed, with the use of a different method, by Dean et al. (1982), although data from a few cells in their study are consistent with linear temporal summation. More recently, Mancini et al. (1990) have analyzed the temporal response properties of simple cells with the use of a white noise method. Their data show that a linear prediction of the temporal impulse response accounts reasonably well, but not completely, for the measured response to a flashing bar stimulus. In addition, Mancini et al. (1990) find a nonlinear response component that may be accounted for by a static nonlinearity, such as a response threshold (see Tadmor and Tolhurst 1989). Mancini et al. conclude, on the basis of data from a small sample of neurons, that temporal summation within simple cells is approximately linear.

Given the disparate nature of these previous findings and the importance of their implications, we have reassessed the nature of temporal summation for a large population of simple cells from the striate cortex of cats and kittens. We have also examined spatial summation for these same cells, to compare temporal and spatial summation with regard to linearity. The approach we have taken is to compare measured spatial and temporal frequency tuning curves for simple cells with linear predictions on the basis of measure-

ments of the spatiotemporal receptive-field profile. Spatial and temporal frequency tuning curves are measured in traditional fashion by the use of drifting sinusoidal gratings. Spatiotemporal receptive-field profiles are obtained by the use of the reverse correlation technique (Jones and Palmer 1987a; McLean and Palmer 1989; Palmer et al. 1991), as described in detail in the companion paper (DeAngelis et al. 1993).

Consistent with previous studies, we find that measured and predicted spatial frequency tuning curves agree well for most simple cells, suggesting that spatial summation is approximately linear. In addition, we find that measured and predicted temporal frequency tuning curves also match well for most cells. Thus we conclude that temporal summation in simple cells is also approximately linear. When measured and predicted tuning curves differ substantially, the largest errors are often manifested at low frequencies. Linear predictions of optimal spatial and temporal frequencies, as well as high spatial and temporal frequency cutoffs, are found to be fairly accurate, confirming the validity of the techniques used in the companion paper (see Figs. 11–13 of DeAngelis et al. 1993).

If simple cells behave as linear spatiotemporal filters, it should also be possible to predict their direction selectivity on the basis of the organization of the spatiotemporal receptive field (i.e., Adelson and Bergen 1985; Watson and Ahumada 1983, 1985). We have examined this notion by comparing responses to gratings moving in the preferred and opposite directions with linear predictions. In agreement with previous work (Albrecht and Geisler 1991; Reid et al. 1987, 1991; Tolhurst and Dean 1991), we find that linear predictions correctly estimate the preferred direction of motion but consistently underestimate the strength of the directional selectivity. In concordance with the recent work of Albrecht and Geisler (1991), we find that the agreement between measured direction selectivity indexes and linear predictions can be markedly improved by accounting for the expansive exponential nonlinearity revealed in the contrast response function.

Overall, our findings show that the spatiotemporal receptive-field profiles of simple cells can be used to predict a variety of response properties with reasonably good accuracy. The adequacy of a linear spatiotemporal filter model for simple cells is discussed with regard to some known nonlinear mechanisms of cortical function. Our results are consistent with recent theoretical efforts in which simple cells are modeled as linear spatiotemporal filters, combined with an expansive nonlinearity and a contrast normalization scheme (Albrecht and Geisler 1991; Heeger 1991, 1992a,b).

METHODS

Most of the methods used in this study are described in the companion paper (DeAngelis et al. 1993), with a couple of exceptions. Contrast response functions were obtained with the use of sinusoidal luminance gratings of optimal orientation and spatial frequency, which drifted in the preferred direction for each neuron. Details of stimulus presentation for the contrast-response measurements are identical to those described in the companion paper for orientation and spatial frequency tuning measurements. Spatial and temporal frequency tuning curves were fit (see Fig. 5)

with appropriate functions (*Eqs. 1* and *2*), with the use of the Simplex method (see Press et al. 1988) to minimize a squared error term.

RESULTS

In the companion paper, we have analyzed the spatiotemporal receptive-field structure of 233 simple cells, recorded from either adult cats or kittens. For 118 of these cells (24 from adult cats, 63 from 8-wk-old kittens, and 31 from 4-wk-old kittens), we have also measured the spatial and temporal frequency selectivity with the use of sinusoidal gratings drifting in the preferred direction for each neuron. In this paper we report an analysis of these 118 cells in which we compare measured spatial and temporal frequency tuning curves with predicted tuning curves obtained through Fourier analysis of the spatiotemporal receptive-field (*X-T*) profile.

Figure 1 illustrates the method by which the responses to gratings are compared with linear predictions on the basis of reverse correlation data. The peristimulus time histograms (PSTHs) of Fig. 1*A* show the responses of a typical simple cell to drifting gratings of varying spatial frequency (*left*) and temporal frequency (*right*). The largest response for this cell is obtained with a spatial frequency of 0.18 cycles/deg and a temporal frequency of 4 Hz. This can be seen more clearly in *D*, where average response rate is plotted as a function of spatial frequency and temporal frequency (see filled circles). Error bars denote ± 1 SE.

Predicted spatial and temporal frequency tuning curves for this cell are obtained through Fourier analysis of the *X-T* profile, which is shown in Fig. 1*B*. A two-dimensional Fast Fourier Transform (FFT) is applied to the *X-T* data, yielding the spatiotemporal amplitude spectrum shown in Fig. 1*C*. By convention, positive temporal frequencies correspond to movement in the neuron's preferred direction; negative temporal frequencies correspond to movement in the opposite (null) direction. To obtain predicted spatial and temporal frequency tuning curves, we first find the peak amplitude in the spatiotemporal frequency spectrum. This is shown by the intersection of the cross-hairs in Fig. 1*C*. By slicing through this peak parallel to the spatial frequency axis, we obtain a predicted spatial frequency tuning curve. Similarly, a slice parallel to the temporal frequency axis gives a predicted tuning curve for temporal frequency. These predicted tuning curves are shown in Fig. 1*D* (—), along with the measurements obtained with the use of gratings. Note that the predicted tuning curves have been scaled (along the *y*-axis) to match the peak response rate from the grating measurements. The predicted curves have not been shifted horizontally or otherwise transformed. For this cell, there is a good agreement between the measured and predicted tuning curves. We may conclude, therefore, that this simple cell sums its inputs approximately linearly over space and time. As a result, the *X-T* profile may be considered a good approximation to the cell's spatiotemporal impulse response function.

Figures 2 and 3 show data for six more simple cells that exhibit a good match between measured and predicted spatial and temporal frequency tuning curves. For each cell the spatiotemporal receptive-field profile is shown as a contour

map (*left*), responses to drifting gratings are shown as filled symbols, and predicted tuning curves based on the assumption of linearity are shown as solid lines. For the cell of Fig. 2*A*, a second set of predicted tuning curves is shown by the dashed lines; these curves were derived by analyzing a second *X-T* profile that was obtained 3 h after the initial measurement. Note that there is excellent agreement between the two sets of predicted tuning curves in Fig. 2*A* (— and ---). In general, we find a very strong correlation between data obtained from repeated measurements of the *X-T* profile (this point is addressed in Fig. 8, *A* and *B*).

All of the cells in Figs. 2 and 3 exhibit band-pass tuning for spatial frequency, with the possible exception of the cell shown in Fig. 2*C*. In this case the grating measurements (filled symbols) do not show a low-frequency rolloff, although a band-pass tuning is suggested by the linear prediction (—). Similarly, most cells show band-pass tuning for temporal frequency when tested with drifting gratings. However, Fig. 3, *B* and *C*, shows temporal frequency data (filled symbols) for two cells that do not exhibit any appreciable low-frequency rolloff when tested with gratings. For these cells, the predicted temporal frequency tuning (—) also shows a low-pass characteristic. This corresponds with the fact that the *X-T* profiles for these cells are approximately unimodal with respect to time. If the impulse response (*X-T* plot) is bimodal or multimodal in time (e.g., Figs. 2*A* and 3*A*), then the predicted temporal frequency tuning curve will always have a band-pass nature.

Most of the cells we have examined show a reasonably good agreement between measured spatial and temporal frequency tuning curves and those predicted on the basis of linear summation. However, many cells do exhibit some systematic deviations from linearity. Figure 4 shows data from three cells for which measured and predicted tuning curves match quite poorly. For the cell shown in Fig. 4*A*, the predicted temporal frequency tuning curve matches well with the responses to gratings; however, the predicted spatial frequency tuning curve is too broad. In this case the error occurs almost exclusively at low spatial frequencies. For high spatial frequencies, the predicted tuning curve agrees well with the responses to gratings. For the cell shown in Fig. 4*B*, the predicted spatial frequency tuning curve matches well with the measured responses, but the predicted temporal frequency tuning curve is much too broad. Again, the error is manifested predominantly at low frequencies. Figure 4*C* shows an example for which both the spatial and temporal frequency predictions are too broad. Because the data are plotted on a logarithmic scale, error at low spatial and temporal frequencies is exaggerated, and error at high frequencies is deemphasized. However, when the data of Fig. 4*C* are plotted on linear frequency axes (not shown), it becomes clear that the predicted tuning curves are broader than the measured data at both low and high frequencies. This pattern of deviation from linearity is common in our sample of neurons.

Quantitative evaluation of linear predictions

So far, we have only examined the adequacy of linear predictions in a qualitative way. We now turn to a quantitative assessment of linearity, which is based on extracting

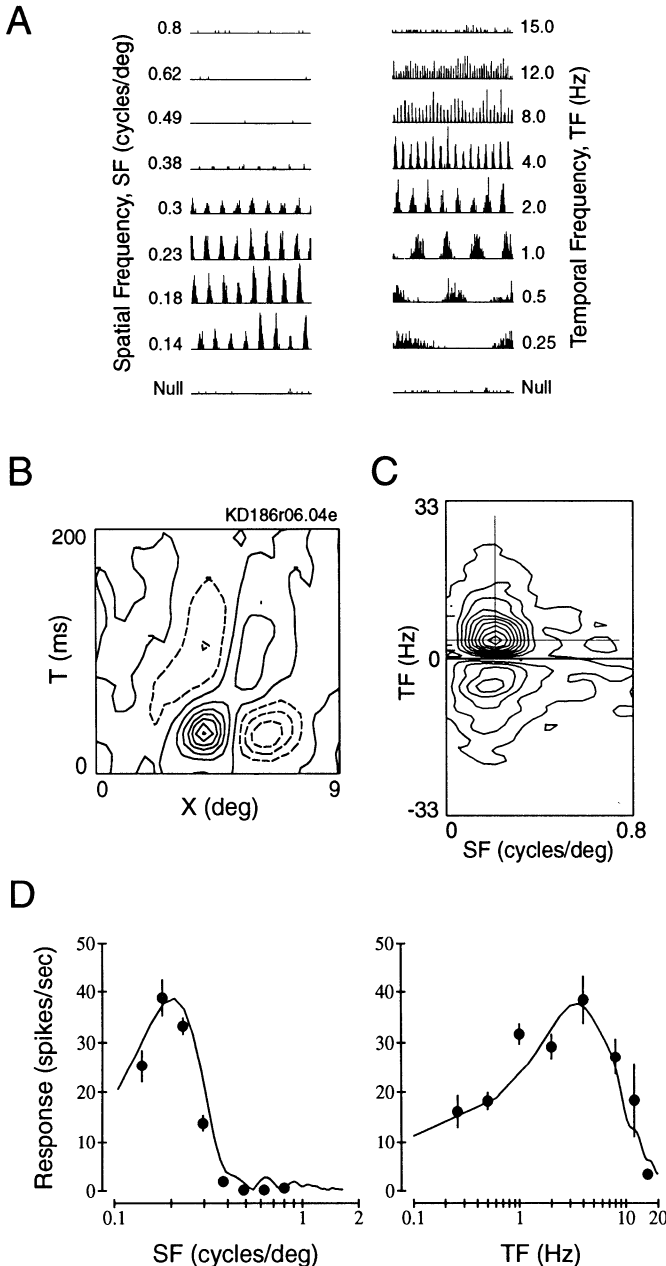


FIG. 1. *A*: comparison is shown between measured spatial and temporal frequency tuning curves and linear predictions obtained from the spatiotemporal receptive-field profile. *A*: responses of a typical simple cell from an adult cat to drifting sinusoidal gratings, which have variable spatial frequency (SF; *left*) or temporal frequency (TF; *right*), are shown as peristimulus time histograms (PSTHs). Each PSTH spans 4 s. For the *left column of histograms*, temporal frequency is fixed at 2 Hz, spatial frequency is varied from 0.14 to 0.8 cycles/deg, and contrast is 20%. For the *right column of histograms*, spatial frequency is fixed at 0.2 cycles/deg, and temporal frequency is varied from 0.25 to 15.0 Hz. Note that the responses are modulated at the temporal frequency of the drifting grating, which is typical of simple cells. *B*: space-time (*X-T*) receptive-field profile is shown for the same cell from which the grating data of *A* were obtained. The *X-T* profile spans 9° of visual space and 200 ms of time. Details of the construction of *X-T* profiles are given in the companion paper (DeAngelis et al. 1993). Solid contours denote bright-excitatory (or ON) subregions; dashed contours denote dark-excitatory (or OFF) subregions. *C*: spatiotemporal amplitude spectrum that is obtained by applying a 2-dimensional Fast Fourier Transform (FFT) to the *X-T* profile shown in *B* (details of the FFT methods are given in the companion paper). Only 2 quadrants of the amplitude spectrum, corresponding to positive spatial frequencies, are shown. This contour map shows response amplitude plotted as a function

parameters from each spatial and temporal frequency tuning curve. To make quantitative comparisons, we first fit the grating data with appropriate curves, as shown in Fig. 5. For the spatial frequency tuning curve (Fig. 5*A*), grating measurements are fit with a Gaussian of the form

$$G(sf) = K e^{-[(sf - sf_0)/a]^2} \quad (1)$$

where K , sf_0 , and a are free parameters, and sf denotes spatial frequency. Note that this function is Gaussian shaped on a linear spatial frequency axis. In Fig. 5*A*, the spatial frequency tuning curve obtained with the use of gratings is shown by filled symbols and the best-fitting Gaussian is shown by the solid curve (plotted on a logarithmic spatial frequency axis). From this best-fitting Gaussian, three parameters are extracted: SF_{opt} , the optimal spatial frequency; SF_{high} , the high spatial frequency cutoff; and SF_{low} , the low spatial frequency cutoff. SF_{opt} is defined as the spatial frequency at which the curve has its peak amplitude, whereas SF_{high} and SF_{low} are defined as the high and low spatial frequencies, respectively, at which the curve drops to one-half of its peak amplitude. If the best-fitting curve does not have enough low-frequency attenuation to reach one-half of the peak amplitude, SF_{low} is assigned a value of zero.

An analogous fitting procedure is carried out for the temporal frequency tuning curve, as illustrated in Fig. 5*B*. In this case the grating data are fit by a gamma distribution having the form

$$G(tf) = K \frac{c(tf - tf_0)^n e^{-[c(tf - tf_0)]}}{n^n e^{(-n)}} \quad (2)$$

where K , c , tf_0 , and n are free parameters, and tf denotes temporal frequency. Three temporal frequency tuning parameters (TF_{opt} , TF_{high} , and TF_{low}) are defined in exactly the same way as described above for the spatial frequency parameters. The reasons for choosing a Gaussian and a gamma distribution to fit the spatial and temporal frequency tuning curves, respectively, are given in the companion paper (DeAngelis et al. 1993). It should be noted that these formulations provide an excellent fit to spatial and temporal frequency tuning data for the vast majority of cells that we have examined. The data shown in Fig. 5 are actually quite typical of the quality of fits obtained.

To compare tuning parameters extracted from grating measurements (as shown in Fig. 5) with tuning parameters extracted from linear predictions, a similar fitting procedure is applied to the spatiotemporal amplitude spectrum obtained through Fourier analysis of the *X-T* profile. This fitting procedure is described in detail in the companion paper (see Fig. 11 and Eq. 5 of DeAngelis et al. 1993) and will not be addressed further here. Note, however, that the same tuning parameters (SF_{opt} , SF_{high} , SF_{low} , TF_{opt} , TF_{high} , TF_{low}) can be extracted from the best fit to the amplitude spectrum. This allows us to make quantitative comparisons

of spatial frequency (SF) and temporal frequency (TF). The intersection of the cross-hairs indicates the peak amplitude in this frequency domain. *D*: superposition of measured and predicted tuning curves. Filled symbols represent the mean firing rates obtained from the PSTHs shown in *A*. Error bars around the responses indicate ± 1 SE. Solid curves show the predicted tuning curves obtained by taking cross sections through the peak of the amplitude spectrum shown in *C*. Note the excellent agreement between the measured and predicted tuning curves.

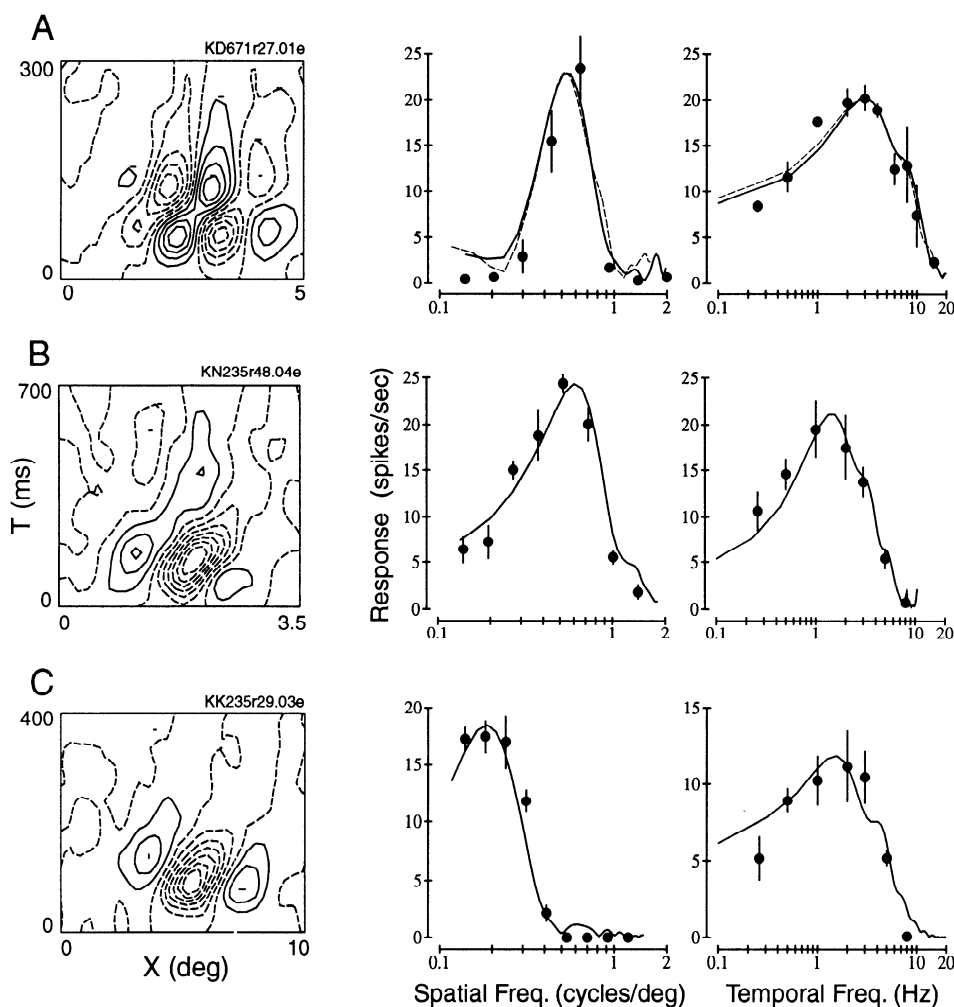


FIG. 2. Evaluation of linearity of spatial and temporal summation is presented for 3 simple cells (*A–C*). For each cell, the space-time (*X-T*) receptive-field profile is shown on the left. Measured spatial and temporal frequency tuning curves are shown on the right as filled circles (error bars, ± 1 SE), and predicted tuning functions are shown as solid curves. For cell *A*, 2 sets of predicted tuning curves are shown (— and ---). These were obtained from 2 separate measurements of the *X-T* profile, separated in time by 3 h. Cell *A* is from an adult cat, cell *B* is from an 8-wk-old kitten, and cell *C* is from a 4-wk-old kitten. All 3 cells exhibit approximately linear spatial and temporal summation.

between measured and predicted tuning curves for a population of cells.

Figure 6 shows a comparison of temporal frequency tuning parameters obtained from grating data and from spatio-temporal receptive-field profiles (via Fourier analysis). In Fig. 6*A*, values of TF_{opt} measured with gratings (vertical axis) are plotted against predictions of TF_{opt} obtained through FFT analysis of the *X-T* profile (horizontal axis). Each point in Fig. 6*A* represents one neuron; circles denote simple cells from adult cats ($n = 24$), squares denote cells from 8-wk-old kittens ($n = 63$), and triangles represent neurons from 4-wk-old kittens ($n = 31$). The diagonal line of slope = 1 represents the prediction based on linearity; if simple cells exhibit linear temporal summation, then the points should be clustered around the diagonal. The shaded region defines the area within which the measured and predicted values of TF_{opt} differ by no more than 50%. Note that the vast majority of points are contained within the shaded region, and that most of the points cluster around the diagonal. Linear regression yields a correlation coefficient of 0.77, which is significant ($F_{1,116} = 172.5$, $P < 0.001$). The regression line (not shown) has a slope of 0.84 and an intercept of 0.61 Hz.

Figure 6*B* shows the relationship between estimates of TF_{high} derived from grating and reverse correlation measurements. Nearly all points fall within the shaded region (<50% error). There is a weak trend for predicted values of

TF_{high} to be slightly larger than measured values. The average predicted value of TF_{high} is 5.54 Hz, and the average measured value of TF_{high} is 5.29 Hz, but this difference is not statistically significant ($P = 0.38$). The coefficient of correlation for the data of Fig. 6*B* is 0.83, which is highly significant ($F_{1,116} = 265.4$, $P < 0.001$). The regression line (not shown) has a slope of 0.88 and an intercept of 0.48 Hz.

Whereas measured and predicted values agree quite well for TF_{opt} and TF_{high} , Fig. 6*C* shows that there is a poor correspondence between these two measurements for TF_{low} . There is a strong tendency for linear predictions of TF_{low} to be too small, such that most points lie above the diagonal in Fig. 6*C*. The average predicted value of TF_{low} is 0.28 Hz, whereas the average measured value of TF_{low} is 0.60 Hz. This difference is highly significant ($P < 0.001$). The coefficient of correlation for the data of Fig. 6*C* is 0.56, which is significant ($F_{1,116} = 50.8$, $P < 0.001$); however, very few points lie within the shaded region representing <50% error. The regression line (not shown) has a slope of 1.09 and an intercept of 0.31 Hz. Overall, the data of Fig. 6 show that linear predictions of the optimal frequency and high-frequency cutoff are reasonably accurate, whereas predictions of the low-frequency cutoff are consistently too small.

A similar conclusion can be drawn from analysis of measured and predicted spatial frequency tuning curves, as summarized in Fig. 7. The format of Fig. 7 is identical to that of

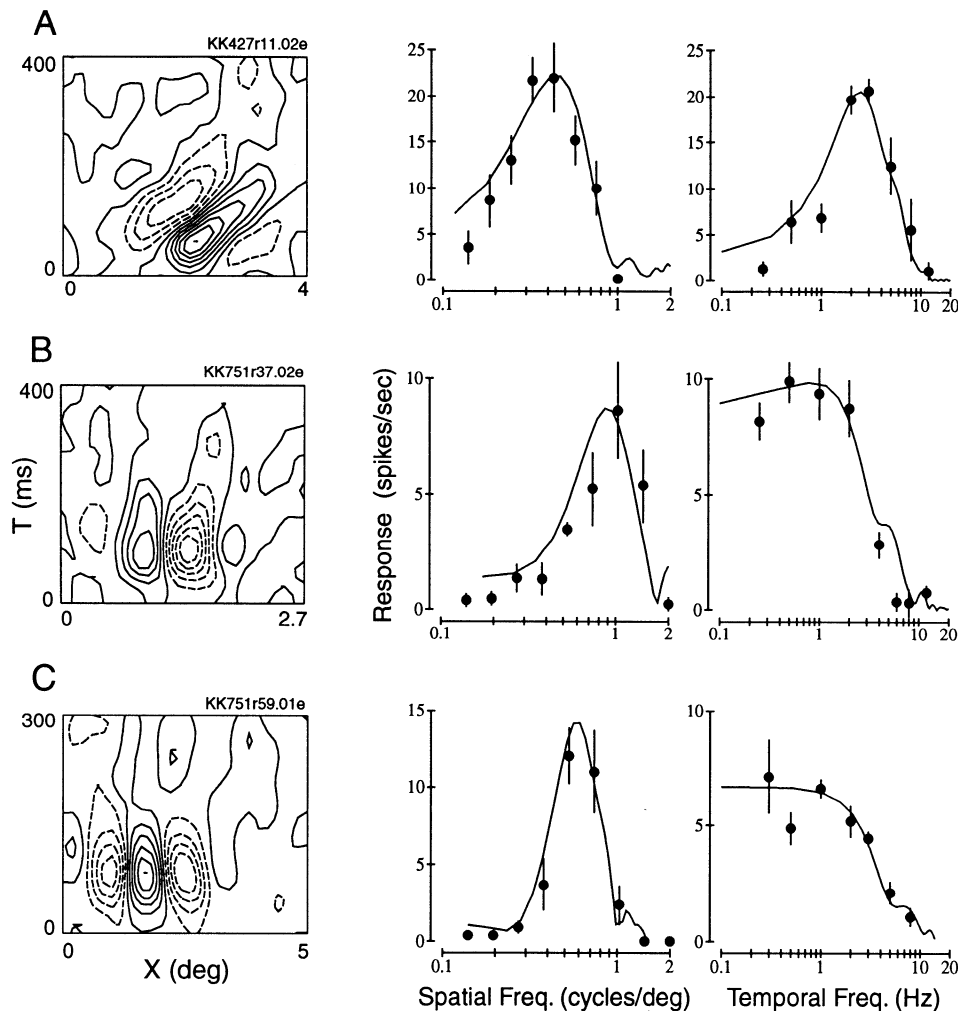


FIG. 3. Comparisons of measured tuning curves and linear predictions are shown for 3 additional cells that exhibit linear spatial and temporal summation. The format is the same as that of Fig. 2. Cell A is from a 4-wk-old kitten; cells B and C are from an 8-wk-old kitten.

Fig. 6, with grating measurements plotted on the vertical axis and linear predictions plotted on the horizontal axis. Figure 7A shows the relationship between measured and predicted values of the optimal spatial frequency (SF_{opt}). Virtually all points fall within the shaded region, and the correlation coefficient is 0.97, which is highly significant ($F_{1,116} = 1,953.8, P < 0.001$). The best-fitting straight line to the data (not shown) has a slope of 1.06 and an intercept of 0.006 cycles/deg. The average value of SF_{opt} from grating measurements (0.42 cycles/deg) is slightly higher than the average value of SF_{opt} obtained from reverse correlation data (0.39 cycles/deg), but the difference is not statistically significant ($P = 0.34$).

Figure 7B shows the relationship between measured and predicted values of the high spatial frequency cutoff, SF_{high} . Again, most points are clustered closely around the diagonal. The coefficient of correlation is 0.95, which is highly significant ($F_{1,116} = 941.7, P < 0.001$). The regression line (not shown) has a slope of 0.97 and an intercept of -0.02 cycles/deg. The average predicted value of SF_{high} (0.66 cycles/deg) is somewhat higher than the average measured value (0.61 cycles/deg), but the difference is not significant ($P = 0.33$).

As for the low temporal frequency cutoff (see Fig. 6C), the correspondence between measured and predicted values of the low spatial frequency cutoff, SF_{low} , is poor (see

Fig. 7C). Although there is a significant correlation ($r = 0.90; F_{1,116} = 588.9, P < 0.001$), the linear predictions are consistently too low (i.e., most points lie well above the diagonal in Fig. 7C). The average predicted value of SF_{low} is 0.14 cycles/deg, whereas the average measured value of SF_{low} is 0.22 cycles/deg; this difference is significant ($P < 0.001$). The regression line for these data (not shown) has a slope of 1.28 and an intercept of 0.05 cycles/deg.

Comparison of Figs. 6 and 7 shows that the overall pattern of correspondence between grating measurements and linear predictions is similar for temporal frequency parameters and spatial frequency parameters. In both cases, estimates of the optimal frequency and high-frequency cutoff obtained from the X - T profile are reasonably accurate. This finding validates the results reported in the companion paper (DeAngelis et al. 1993), in which linear predictions of TF_{opt} , TF_{high} , SF_{opt} , and SF_{high} are used to gauge the postnatal development of spatial and temporal frequency selectivity in kittens. Low-frequency cutoff values obtained from the X - T profile are typically not accurate, however. Note that this does not impact the results reported in the companion paper, because low-frequency cutoff values were not used. Note also that there are no differences between kittens and cats with regard to the data presented in Figs. 6 and 7.

There is one consistent difference between the temporal

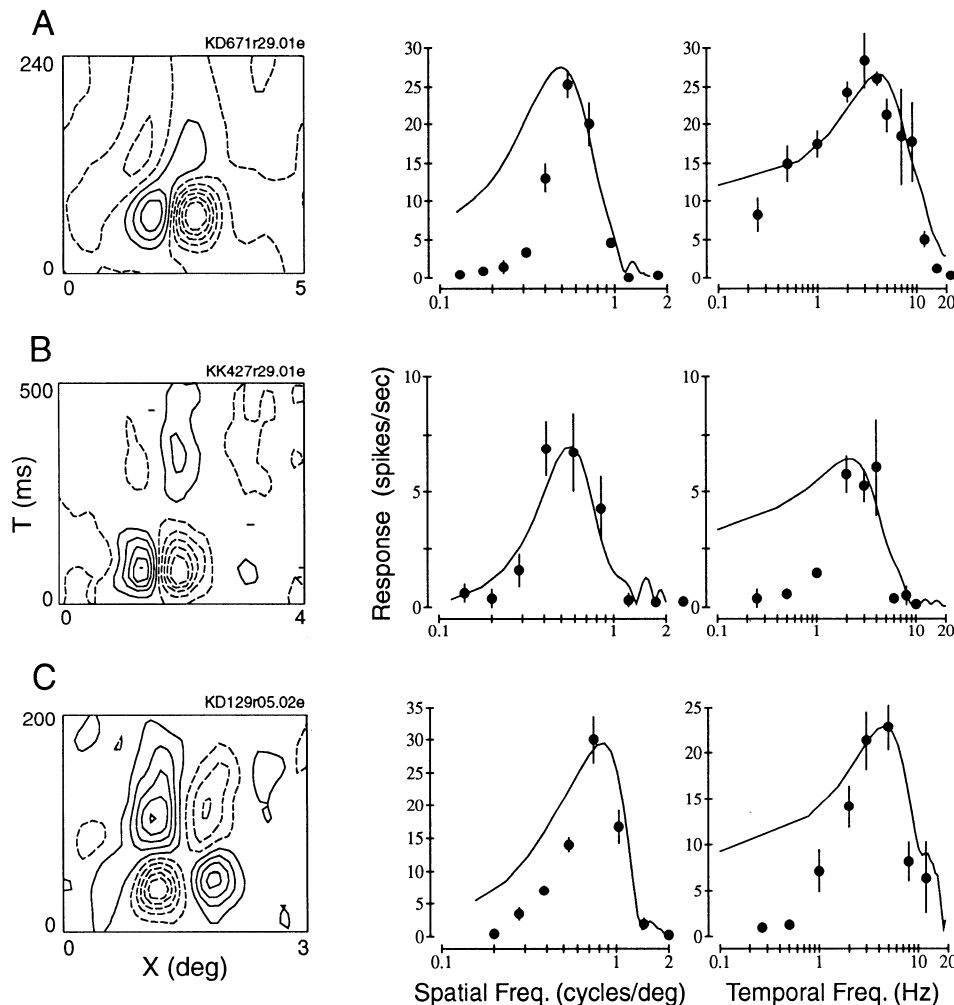


FIG. 4. Measured and predicted tuning curves are shown for 3 cells that exhibit systematic deviations from linearity, as described in the text. Cells A and C are from adult cats; cell B is from a 4-wk-old kitten.

frequency data shown in Fig. 6 and the spatial frequency data shown in Fig. 7. The correlation between measured and predicted values is clearly weaker for temporal frequency parameters than for spatial frequency parameters. This difference is reflected in the correlation coefficients, which are substantially smaller for the temporal frequency data (Fig. 6) than for the spatial frequency data (Fig. 7).

Variability in reverse correlation and grating measurements

As noted above, the correlation between measured and predicted values of tuning parameters is weaker for temporal frequency than for spatial frequency. At first glance, this finding suggests that linear predictions are less reliable for temporal frequency than for spatial frequency. However, this conclusion relies on the assumption that the inherent variability in the temporal frequency tuning measurements is equivalent to the variability in the spatial frequency tuning measurements. We have examined this assumption by comparing parameters obtained from repeated grating and reverse correlation measurements.

We first consider variability in repeated estimates of spatial and temporal frequency tuning parameters obtained from spatiotemporal receptive-field profiles (via Fourier analysis). Figure 8A shows the correlation between estimates of SF_{opt} obtained from repeated measurements of the

X - T profile. If repeat measurements produce identical estimates of SF_{opt} , then all of the data points should fall on the diagonal line of slope = 1. Indeed, the data conform closely to this ideal behavior, because all of the data points are contained well within the shaded region that delineates <50% error. Linear regression yields a correlation coefficient of 0.98 ($F_{1,36} = 1004.5$, $P < 0.001$). The regression line (not shown) has a slope of 0.99 and an intercept of 0.004 cycles/deg. A similar result is shown in Fig. 8B for estimates of TF_{opt} obtained from repeated reverse correlation measurements. Again, estimates of TF_{opt} from repeated trials are highly consistent. In this case the coefficient of correlation is 0.96 ($F_{1,21} = 426.7$, $P < 0.001$); the regression line (not shown) has a slope of 0.96 and an intercept of 0.09 Hz. Overall, the data of Fig. 8, A and B, show that spatial and temporal frequency tuning estimates (i.e., linear predictions) obtained from the spatiotemporal receptive-field profile are highly repeatable.

We have also assessed variability in spatial and temporal frequency tuning measurements obtained with the use of drifting gratings. Figure 8C shows the correlation between estimates of SF_{opt} obtained from repeated measurements of the spatial frequency tuning curve. It is clear that repeat estimates of SF_{opt} obtained with the use of gratings are very consistent, as indicated by the correlation coefficient of 0.97 ($F_{1,36} = 381.8$, $P < 0.001$) in Fig. 8C. Figure 8D

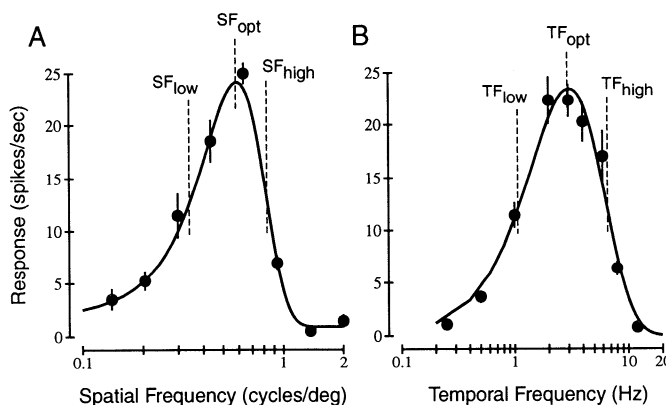


FIG. 5. Fitting procedure used to extract tuning parameters for quantitative analyses. *A*: measured spatial frequency tuning is shown for a simple cell from an adult cat. Average firing rates in response to drifting gratings of various spatial frequencies are plotted as filled symbols. Error bars, ± 1 SE for each average response. The solid curve is the Gaussian function (see Eq. 1) which best fits these tuning data. From this fit, 3 spatial frequency parameters are extracted: SF_{opt} , SF_{low} , and SF_{high} , as indicated by the dashed vertical lines (see text). *B*: measured temporal frequency tuning data (filled symbols) and the gamma distribution function (solid curve, see Eq. 2) that best fits the data are presented here for the same simple cell as shown in *A*. Three parameters (TF_{opt} , TF_{low} , and TF_{high}) are extracted from the curve.

shows, however, that estimates of TF_{opt} obtained with the use of gratings are not as repeatable as estimates of SF_{opt} . For TF_{opt} , the correlation coefficient between successive grating measurements is 0.81 ($F_{1,21} = 40.4$, $P < 0.001$), which is similar to the coefficient ($r = 0.77$) obtained from comparing grating and reverse correlation estimates (Fig. 6*A*). Note that the data points in Fig. 8*D* are scattered throughout the shaded region, indicating that values of TF_{opt} from repeat trials can differ by as much as 50%. Figure 8 only shows repeat measurements of the optimal spatial and temporal frequencies, but very similar results are obtained for the high-frequency and low-frequency cutoffs.

If one compares grating measurements with reverse correlation measurements for a population of neurons, the strength of the correlation between the grating data and the reverse correlation data is limited by the variability within each type of measurement. Figure 8, *A* and *C*, shows that estimates of the optimal spatial frequency, SF_{opt} , obtained from either grating measurements ($r = 0.97$) or reverse correlation measurements ($r = 0.98$) are highly repeatable. This permits the correlation between grating and reverse correlation measurements of SF_{opt} to be very strong ($r = 0.97$; see Fig. 7*A*). In contrast, comparison of Fig. 8, *B* with *D*, reveals that estimates of the optimal temporal frequency obtained with the use of gratings are less repeatable ($r = 0.81$) than estimates of TF_{opt} obtained from reverse correlation measurements ($r = 0.96$). As a result, the correlation between grating and reverse correlation measurements of TF_{opt} is not very strong ($r = 0.77$; see Fig. 6*A*). Similar logic applies to the measurement of high- and low-frequency cutoffs. Therefore it appears that the lower correlation coefficients in Fig. 6, as compared with Fig. 7, result from variability in grating measurements of temporal frequency tuning curves, rather than from nonlinearities of temporal summation. It is not clear, however, why grating measurements of temporal frequency tuning parameters should be more

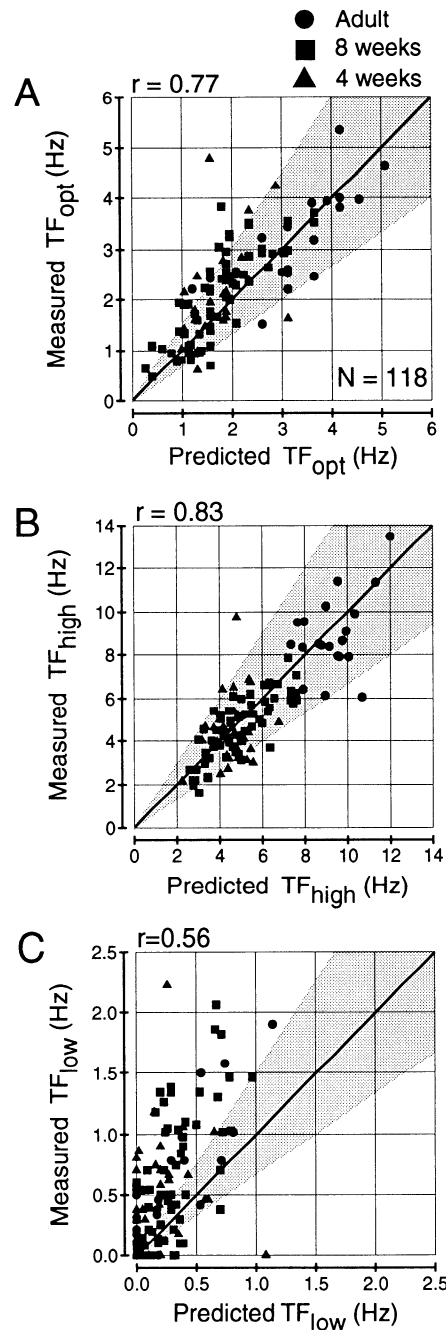


FIG. 6. Quantitative comparison between temporal frequency parameters obtained from measured tuning curves and parameters derived from linear predictions. In each panel, grating data are plotted on the vertical axis, and linear predictions (from reverse correlation data) are plotted on the horizontal axis. *A*: comparison is shown of optimal temporal frequency (TF_{opt}) estimates obtained from grating measurements and linear predictions. Data are presented for a total of 118 simple cells, recorded from adult cats (●), 8-wk-old kittens (■), and 4-wk-old kittens (▲). The diagonal line of unity slope indicates a perfect correspondence between measured and predicted values. The shaded area contains points for which the measured and predicted values differ by <50%. The correlation coefficient is 0.77. *B*: comparison between measured and predicted estimates of the high temporal frequency cutoff (TF_{high}) is displayed here. In this case the correlation coefficient is 0.83. *C*: a scatter plot is given of measured and predicted values of the low temporal frequency cutoff (TF_{low}). Most points lie above the diagonal and outside of the shaded region, indicating a poor correspondence. The correlation coefficient is 0.56.

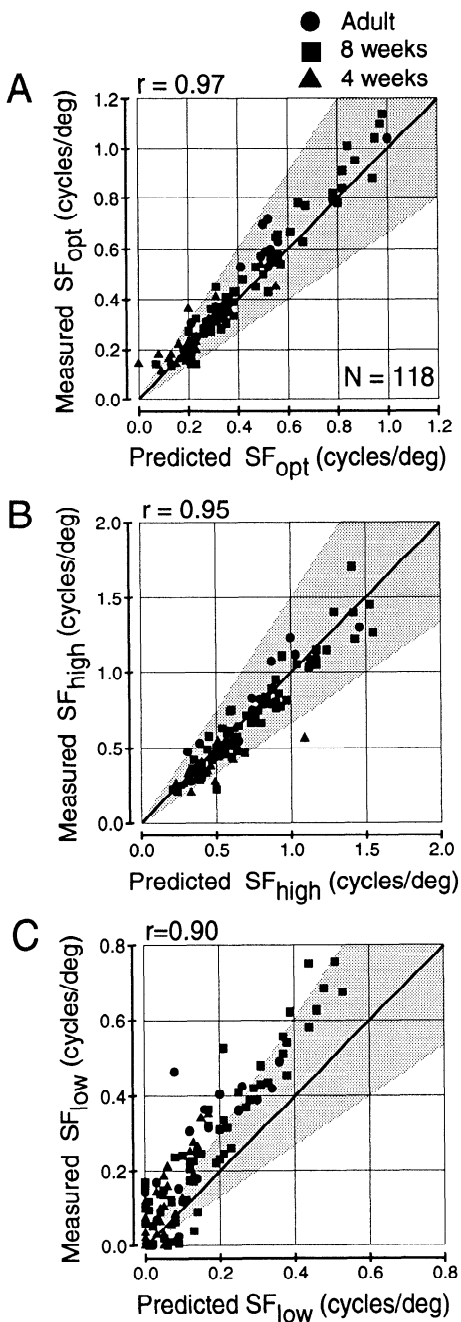


FIG. 7. Quantitative comparisons between measured and predicted spatial frequency tuning parameters are exhibited here. The format is identical to that of Fig. 6. *A*: this scatter plot shows the relationship between measured and predicted values of the optimal spatial frequency (SF_{opt}). A strong correlation ($r = 0.97$) is evident. *B*: a scatter plot showing that linear predictions of the high spatial frequency cutoff (SF_{high}) agree well with measured values ($r = 0.95$). *C*: linear predictions of the low spatial frequency cutoff (SF_{low}) tend to underestimate the measured values, hence most of the points lie well above the diagonal.

variable than grating measurements of spatial frequency tuning parameters.

Direction selectivity

If simple cells behave as linear spatiotemporal filters, then direction selectivity may be predicted from the spatiotemporal impulse response (see for example Adelson and

Bergen 1985; Watson and Ahumada 1983, 1985). Specifically, cells with $X-T$ profiles that are “tilted” in the space-time domain (i.e., space-time inseparable) should exhibit a preference for the direction of motion of a visual stimulus. In the companion paper (DeAngelis et al. 1993) we compute a direction selectivity index (DSI, see *Eq. 7* of the companion paper) from the spatiotemporal amplitude spectrum obtained via Fourier analysis of the $X-T$ profile. Here we compare estimates of DSIs obtained from the $X-T$ profiles with measurements of DSIs made, in traditional fashion, with the use of drifting sinusoidal gratings.

Figure 9 illustrates the analysis of direction selectivity for a typical simple cell. A bi-directional orientation tuning curve for this cell is shown in Fig. 9*A*, where diamonds denote responses to gratings of variable orientation that drift in the preferred direction and squares indicate responses to stimuli moving in the opposite direction. The orientation tuning curve for this cell, and all others, is obtained with the use of gratings of the optimal spatial frequency that drift at a temporal frequency of 2 Hz. The solid curves in Fig. 9*A* are Gaussian functions that best fit the orientation tuning data. Response in the preferred direction, R_p , and response in the nonpreferred direction, R_{np} , are determined by the peak values of the best-fitting Gaussians. The DSI is defined as

$$DSI = \frac{R_p - R_{np}}{R_p + R_{np}} \quad (3)$$

Values of the DSI range from 0.0 (no direction selectivity) to 1.0 (complete direction selectivity). For the cell of Fig. 9*A*, the DSI obtained from grating measurements is 0.79, indicating that the cell is strongly direction selective.

If linearity is assumed, a predicted DSI can be computed from the spatiotemporal receptive-field profile and compared with the DSI measured with the use of gratings. Figure 9*B* shows the $X-T$ profile for the same simple cell from which the grating data of Fig. 9*A* were recorded. Fourier analysis of the $X-T$ data yields the spatiotemporal amplitude spectrum shown in Fig. 9*C*. As noted above, positive temporal frequencies correspond to motion in the preferred direction, and negative temporal frequencies correspond to motion in the nonpreferred direction. To obtain a linear prediction of the DSI, we find the values of the amplitude spectrum corresponding to the motion of a grating having optimal spatial frequency and drifting at a temporal frequency of 2 Hz. These values are indicated by the intersections of the cross-hairs in Fig. 9*C*. R_p is taken to be the value of the amplitude spectrum at a spatial frequency of 0.3 cycles/deg and a temporal frequency of +2 Hz; R_{np} is defined as the amplitude at 0.3 cycles/deg and -2 Hz. From these values, a predicted DSI is computed with the use of *Eq. 3*. The predicted DSI for this cell has a value of 0.43, which is roughly one-half of the value (DSI = 0.79) obtained with gratings. This discrepancy is typical of most cells.

Figure 9*D* shows the predicted DSI (from reverse correlation data) plotted against the measured DSI (from grating data) for a population of 190 simple cells from adult cats and kittens. Each point in this scatter plot represents one neuron. Large positive values of the DSI indicate a strong preference for motion in one direction, whereas negative values indicate a preference for motion in the opposite di-

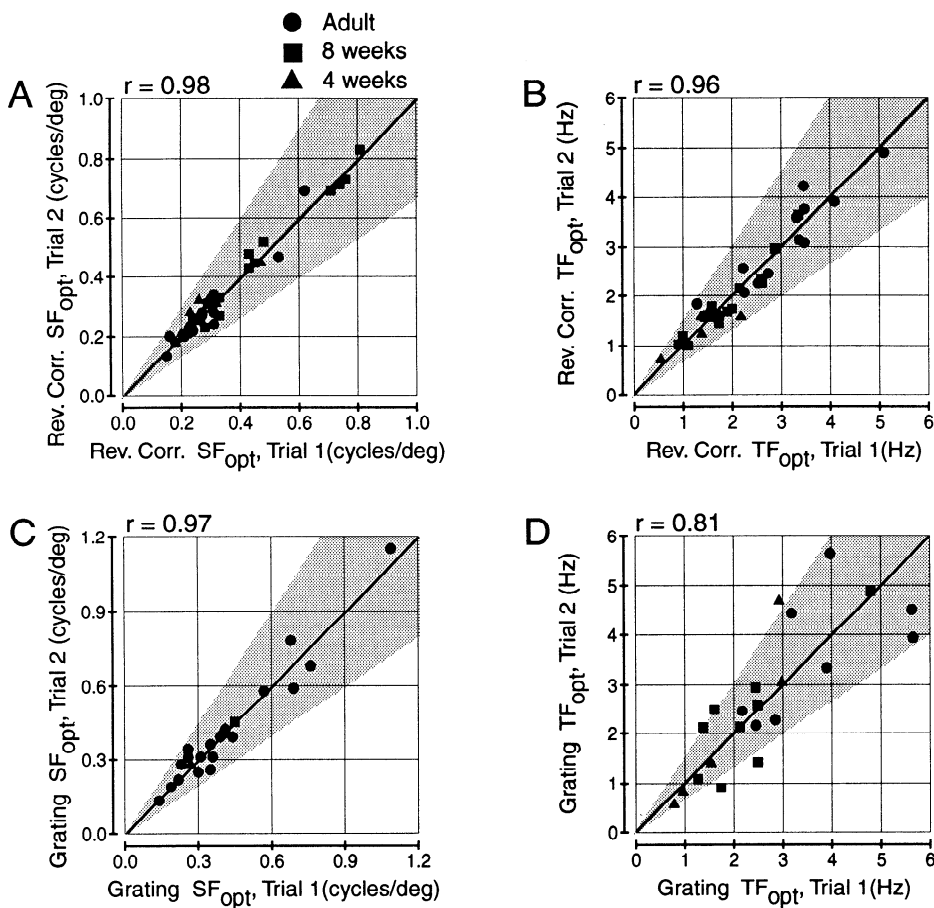


FIG. 8. An evaluation is shown of variability in spatial and temporal frequency tuning parameters obtained from reverse correlation data (*A* and *B*) and from responses to gratings (*C* and *D*). *A*: comparison is made between optimal spatial frequency (SF_{opt}) estimates obtained from repeated measurements of the X - T profile. Each data point represents 1 neuron. For each of these cells, 2 separate measurements of the X - T profile were obtained with the use of the reverse correlation method. Linear predictions of SF_{opt} from the 1st trial are plotted on the horizontal axis, and estimates of SF_{opt} from the 2nd trial are plotted on the vertical axis. Points are clustered tightly around the diagonal line, indicating that estimates of SF_{opt} obtained from reverse correlation data are highly repeatable ($r = 0.98$). *B*: a scatter plot shows the correspondence between estimates of the optimal temporal frequency (TF_{opt}) obtained through Fourier analysis of repeated measurements of the X - T profile. Again, the linear predictions of TF_{opt} are shown to be very repeatable ($r = 0.96$). *C*: comparison between repeat measurements of SF_{opt} obtained with gratings is shown here. For each neuron, 2 separate measurements of the spatial frequency tuning curve were obtained. Values of SF_{opt} from the 1st trial are plotted on the horizontal axis, and values of SF_{opt} from the 2nd trial are plotted on the vertical axis. The correlation is very strong ($r = 0.97$). *D*: comparison of repeated measurements of TF_{opt} obtained with gratings. Comparison of these data with those in *C* shows that there is more variability in repeat measurements of TF_{opt} ($r = 0.81$) than in repeat measurements of SF_{opt} ($r = 0.97$).

rection. The data of Fig. 9*D* show that the reverse correlation data correctly predict the preferred direction of motion for $\sim 95\%$ of the cells tested (i.e., almost all data points lie within the shaded quadrant). For 11 cells the reverse correlation and grating data predict opposite direction preferences; however, the directional indexes for most of these cells are close to 0.0. Because these cells are nearly equally responsive to both directions of motion, a small amount of variability in the response can yield measured and predicted DSIs of opposite sign. For all cells that exhibit a strong directional preference in response to gratings ($DSI > 0.5$), the reverse correlation data correctly predict the preferred direction of motion.

Although the reverse correlation data are accurate in predicting the direction preference of most simple cells, DSI values predicted from the X - T profiles typically *underestimate* the actual DSIs measured with gratings (i.e., most points in Fig. 9*D* lie *below* the diagonal). This means that the actual direction preference is more pronounced than that predicted from the spatiotemporal receptive-field profile. Thus linear predictions of direction selectivity are not accurate. Similar findings have been reported in studies that compare responses to drifting gratings with responses to counterphase modulated gratings (Albrecht and Geisler 1991; Reid et al. 1987, 1991; Tolhurst and Dean 1991). For the data of Fig. 9*D*, linear regression yields a correlation coefficient of 0.64, which is significant ($F_{1,188} = 128.1$, $P < 0.001$). The regression line (shown dashed) has a slope of 0.47 and an intercept of 0.06. There is no significant differ-

ence between kittens and cats with regard to the relationship between measured and predicted values of the DSI. Overall, the DSI predicted on the basis of linearity is approximately one-half as large as the DSI measured with gratings.

Recently, Albrecht and Geisler (1991) have shown that the disparity between linear predictions and measured values of DSIs can be reconciled by accounting for the expansive nonlinearity revealed in the contrast-response function. In the present study we have not measured contrast-response functions as part of the standard experimental protocol; hence we cannot directly test the method of Albrecht and Geisler for the whole population of cells shown in Fig. 9*D*. In a couple of experiments, recently, we have obtained contrast-response data, as well as X - T profiles, for a small group of simple cells. For each of these cells, we have fit the contrast-response data with the use of the method described by Albrecht and Geisler (1991) and Albrecht and Hamilton (1982). This fitting procedure is illustrated in Fig. 10*A* for a representative simple cell. The diamonds show the response of the neuron to drifting sinusoidal gratings of variable contrast from 3 to 60%. The solid curve is the best-fitting function of the form

$$R(c) = \frac{R_{max} c^n}{c^n + c_{50}^n} \quad (4)$$

where R_{max} , n , and c_{50} are free parameters, and c denotes contrast. In this formulation, response [$R(c)$] increases exponentially with contrast for contrasts below the semisaturation coefficient (c_{50}); for contrasts above c_{50} , response be-

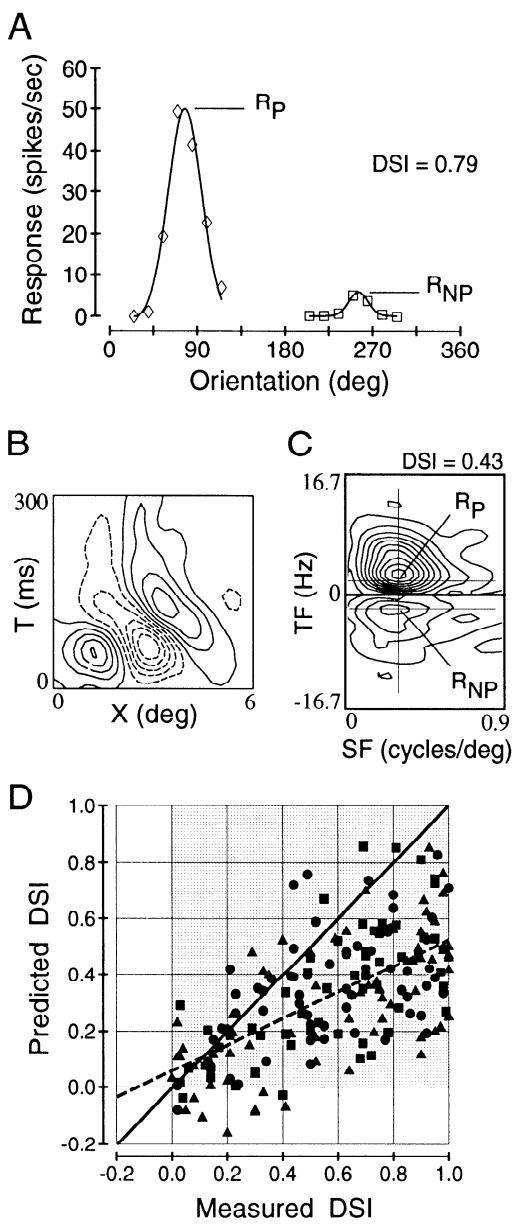


FIG. 9. *A*: comparison between direction selectivity measurements made with the use of gratings and linear predictions is shown here. *A*: traditional direction selectivity measurements are obtained with the use of drifting sinusoidal gratings. This panel shows an orientation tuning curve for a typical simple cell. Seven orientations (15° apart) are tested around the preferred direction of motion (\diamond) and around the opposite direction (\square). Smooth curves show the best-fitting Gaussian functions to these orientation tuning data. A direction selectivity index (DSI) is computed (see Eq. 3) with the use of the peak responses in the preferred (R_p) and nonpreferred (R_{np}) directions. The drifting grating stimulus used for this test had a spatial frequency of 0.3 cycles/deg, a temporal frequency of 2 Hz, and a contrast of 50%. *B*: space-time (X - T) receptive-field profile for the same simple cell. Note that the subregions are clearly tilted toward the left in the space-time domain. *C*: a 2-dimensional Fast Fourier Transform is applied to the X - T data shown in *B* to obtain the spatiotemporal amplitude spectrum, shown here as a contour map. A linear prediction of R_p is obtained by finding the value of the amplitude spectrum at a spatial frequency of 0.3 cycles/deg and a temporal frequency of +2 Hz (indicated by the intersection of the cross-hairs), because these are the parameters of the grating stimulus used to collect the data shown in *A*. Similarly, an estimate of R_{np} is the amplitude at a spatial frequency of 0.3 cycles/deg and a temporal frequency of -2 Hz. From these values, a predicted DSI is computed, with the use of Eq. 3. *D*: in this scatter plot, the DSI measured with gratings is plotted on the horizontal axis, and the predicted DSI (assuming linearity)

gins to saturate rather quickly as a function of contrast. The exponent, n , is taken as a metric of the expansive nonlinearity (see Albrecht and Geisler 1991).

If we assume that the expansive exponent given by the contrast-response function is the only response nonlinearity affecting the output of the simple cell, we can correct the values of the DSI obtained from grating measurements and linear predictions (see APPENDIX). After this correction, the predicted DSI (from reverse correlation data) and the measured DSI should agree, provided that other nonlinearities do not have a significant contribution. Figure 10*B* shows that correcting for the contrast-response nonlinearity eliminates most of the discrepancy between measured and predicted values of the DSI. The open circles in Fig. 10*B* show uncorrected estimates of the direction selectivity index for eight simple cells. As for the larger population of cells shown in Fig. 9*D*, the DSI measured with gratings is consistently larger than the DSI predicted from reverse correlation (\circ). The filled circles in Fig. 10*B* show corrected estimates of the DSI for the same eight simple cells. Note that most of the points now cluster closely around the diagonal, which represents the linear prediction. The average value of the expansive exponent, n , for these cells is 2.28, which is close to the mean value ($n = 2.5$) reported by Albrecht and Hamilton (1982) and Albrecht and Geisler (1991). Thus the data of Fig. 10*B* support the findings of Albrecht and Geisler (1991) (but see DISCUSSION) and show that DSIs can be predicted on the basis of linear spatiotemporal receptive-field structure, if the contrast-response nonlinearity is known.

In Fig. 10, we have used measurements of the expansive exponent nonlinearity to "correct" measured and predicted DSIs. In an alternative approach, we can compute the value of the exponent that is necessary to bring the measured and predicted DSIs into exact correspondence. This computation has been performed for each of the 190 simple cells shown in Fig. 9*D*, and the distribution of computed exponents is shown in Fig. 11*A*. Statistical analysis (Tukey's HSD test) reveals that there is no significant difference between the distributions of exponents for adult cats (■), 8-wk-old kittens (■), and 4-wk-old kittens (□). As a result, we have combined data across these three age groups, as shown in Fig. 11*B*.

Figure 11*C* shows the distribution of exponents measured by Albrecht and Hamilton (1982) for a population of 127 cortical cells from adult cats. These data were obtained by fitting curves to contrast response functions, as illustrated in Fig. 10*A*. Note that the distribution of exponents measured by Albrecht and Hamilton (1982) is strikingly similar to the distribution of computed exponents shown in Fig. 11*B*. In fact, these two distributions are statistically indistinguishable ($\chi^2 = 3.3$; $P = 0.65$). This finding further supports the notion that direction selectivity may be ex-

plotted on the vertical axis. Data are shown for a total of 190 simple cells: 65 from adult cats (●), 55 from 8-wk-old kittens (■), and 70 from 4-wk-old kittens (▲). The diagonal line of unity slope (solid) indicates the ideal behavior of a linear spatiotemporal filter. The dashed line shows the result of linear regression analysis (slope = 0.47, y -intercept = 0.06, $r = 0.64$). Points that lie within the shaded quadrant indicate cells for which linear predictions correctly determine the preferred direction of motion.

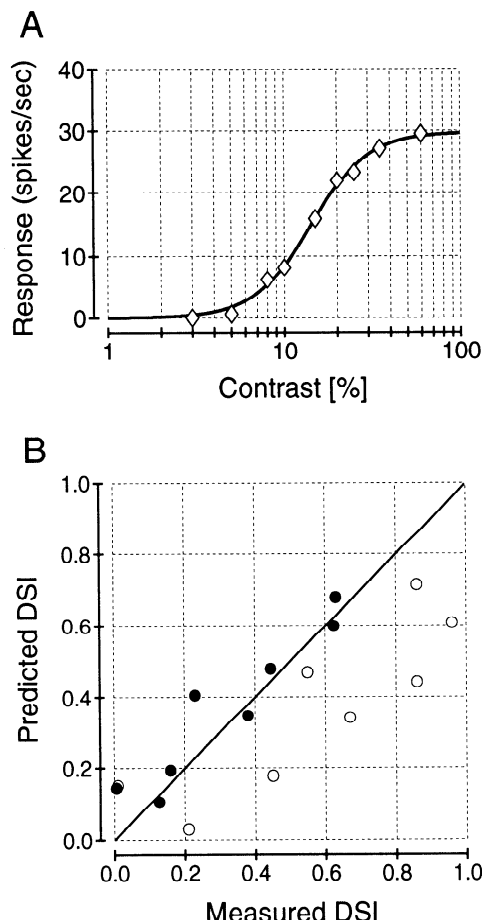


FIG. 10. Correction of direction selectivity estimates based on measurement of the contrast-response nonlinearity. *A*: a contrast response function is shown for a simple cell. Responses to gratings (that have optimal orientation and spatial frequency, and drift at a temporal frequency of 2 Hz) as a function of contrast are indicated by diamonds. The solid curve shows the best fit to these data, as formulated in Eq. 4. For this cell, the expansive exponent, n , has a value of 2.7, and the semisaturation coefficient, c_{50} , has a value of 14.2. *B*: a scatter plot shows the relationship between measured and predicted values of the direction selectivity index (DSI). Open circles show the data for 8 simple cells *before* correction for the expansive exponent nonlinearity. As for the data of Fig. 9*D*, the points generally fall well below the diagonal. Filled circles show the data for these same 8 neurons *after* correction for the expansive nonlinearity. Note that the filled circles cluster closely around the diagonal.

plained by the combination of a linear spatiotemporal filter and a static (i.e., exponent) nonlinearity.

DISCUSSION

For a linear filter, the magnitude of the response to sinusoidal inputs (i.e., the modulation *transfer function*) can be predicted from the responses to very narrow pulse inputs (i.e., the *impulse response*). We have evaluated the linearity of spatial and temporal summation in simple cells by comparing the responses to drifting sinusoidal-luminance gratings with linear predictions computed from spatiotemporal receptive-field profiles. Our main findings are as follows. 1) For most cells, measured spatial frequency tuning curves match fairly well with linear predictions. However, there is some tendency for predicted spatial frequency tuning curves to be too broad. These results are generally consistent with previous work (Andrews and Paffen 1979; De-

Valois et al. 1978; Glezer et al. 1980, 1982; Kulikowski and Bishop 1981a; Maffei et al. 1979; Movshon et al. 1978; Tadmor and Tolhurst 1989; Webster and DeValois 1985). 2) For most cells, measured temporal frequency tuning curves match reasonably well with linear predictions. Again, deviations from linearity are manifested in predicted tuning curves that are too broad. In some cases, linear predictions differ from measured tuning curves *only* at low spatial and temporal frequencies. 3) Linear predictions are accurate for determining the preferred direction of motion for virtually all cells. However, linear predictions typically *underestimate* the strength of directional selectivity by about a factor of two. This result is similar to those reported

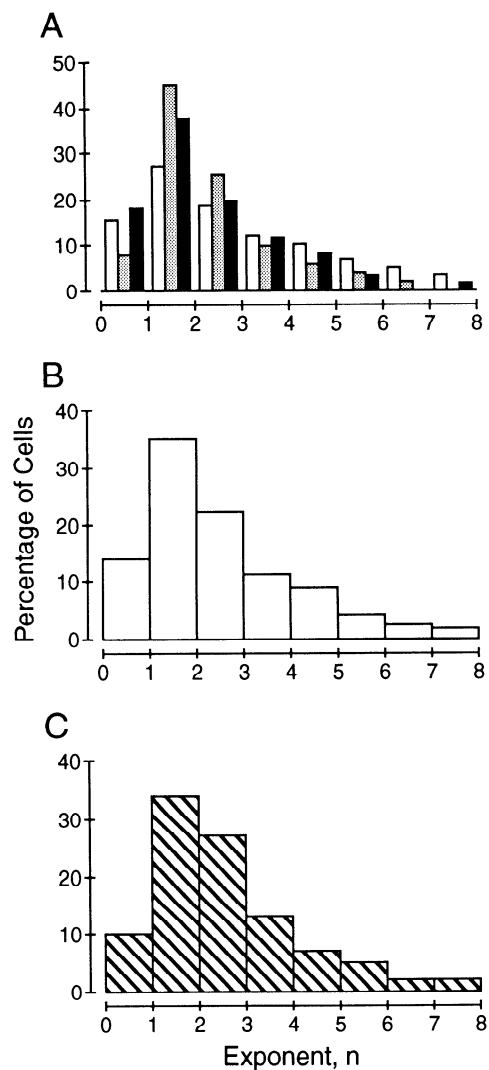


FIG. 11. Distributions are shown of exponent values required to bring measured and predicted values of the direction selectivity index into correspondence (i.e., to make all the data points of Fig. 9*D* fall exactly on the diagonal line). *A*: the distribution of computed exponents (n) for the population of 190 simple cells shown in Fig. 9*D*. Data for cells from adult cats, 8-wk-old kittens, and 4-wk-old kittens are shown as black, gray, and white bars, respectively. The distributions of n for the 3 age groups are not significantly different. *B*: histogram shows the distribution of n for all simple cells ($n = 190$), combined across the 3 age groups. The mean value of n is 2.4. *C*: histogram here (▨) shows the distribution of exponents measured by Albrecht and Hamilton (1982) for a population of 127 cells from the striate cortex of adult cats. The mean of this distribution is 2.5. Note that this distribution is nearly indistinguishable from that shown in *B*.

previously in studies that used a different method (Albrecht and Geisler 1991; Reid et al. 1987, 1991; Tolhurst and Dean 1991). Compensation for the expansive nonlinearity revealed in the contrast-response function reconciles the disparity between measured DSIs and linear predictions, as previously reported by Albrecht and Geisler (1991).

Overall, our findings are consistent with the notion that simple cells sum their inputs approximately linearly over space *and* time. Some of our results are also consistent with the idea that linear summation is followed by a static (output) nonlinearity (Albrecht and Geisler 1991; Andrews and Pollen 1979; DeValois et al. 1985; Heeger 1991; Kulikowski and Bishop 1981a; Mancini et al. 1990; Tadmor and Tolhurst 1989). As discussed below, several other types of nonlinearities are known to modulate the response properties of simple cells. Nevertheless, our data show that these nonlinearities do not severely affect the accuracy of linear predictions based on the spatiotemporal receptive-field profile. $X\text{-}T$ profiles obtained from simple cells by the use of reverse correlation can be used to predict, with reasonable accuracy, a variety of response properties, including spatial and temporal frequency tuning. These results validate the methodology used in the companion paper (DeAngelis et al. 1993).

Temporal summation

Results of several previous studies have suggested that spatial summation in simple cells is approximately linear (Andrews and Pollen 1979; DeValois et al. 1978; Glezer et al. 1980, 1982; Kulikowski and Bishop 1981a; Maffei et al. 1979; Movshon et al. 1978; Tadmor and Tolhurst 1989; Webster and DeValois 1985). Our findings are generally consistent with these results. With regard to linearity of temporal summation, previous studies (Dean et al. 1982; Mancini et al. 1990; Tolhurst et al. 1980) have reached widely differing conclusions. Tolhurst et al. (1980) report that linear predictions of the temporal frequency tuning curve, obtained through Fourier analysis of the response to a flashed grating, match very poorly with measured temporal frequency tuning curves. Thus they conclude that temporal summation in simple cells is grossly nonlinear. In contrast, Mancini et al. (1990) have analyzed the temporal response properties of simple cells with the use of a white noise technique, and they conclude that temporal summation within simple cells is approximately linear.

We have taken a similar approach to that used by Tolhurst et al. (1980), namely comparing measured temporal frequency tuning curves with linear predictions, but our findings are more in accord with those of Mancini et al. (1990) than with those of Tolhurst et al. (1980). These differences may be attributed primarily to methodological considerations. In our reverse correlation experiments, simple cells are stimulated with a long, pseudorandom sequence of briefly flashed (i.e., 40-ms duration) bar stimuli (see Fig. 2 of the companion paper, DeAngelis et al. 1993). The response of most cells under these conditions is a steady, unpatterned discharge at a mean rate of a few spikes per second. Qualitatively, the response is similar to the maintained discharge of cortical cells that fire spontaneously (such as some complex cells). Thus during the course

of a reverse correlation run most simple cells are operating at an approximately steady-state response level that is well within their dynamic range. The appearance or disappearance of a single bar stimulus produces only a small modulation of the cell's response, on top of a relatively constant state of ongoing neuronal activity. A similar type of response is undoubtedly obtained during white noise experiments, as noted by Mancini et al. (1990).

In contrast, the predicted temporal frequency tuning curves of Tolhurst et al. (1980) are obtained through analysis of the response to a grating that is flashed on for 2 s. This yields a "step response" that is differentiated to obtain an impulse response; the impulse response is subsequently Fourier transformed to obtain a predicted temporal frequency tuning curve. In this situation, the neuron is quiet before the stimulus, produces a large transient response at the onset of the stimulus, and subsequently exhibits some sustained discharge during the remainder of the stimulus presentation. This paradigm induces a large change in the operating point of the cell being recorded, as well as changes in operating point for many nearby cells that may interact with the recorded cell. This large disturbance may reveal nonlinearities in the cortical neuronal network (e.g., the rapid contrast gain control described by Bonds 1991) that are not stimulated in our experiments.

An engineering analogy may help to clarify the differences between our experimental paradigm and that of Tolhurst et al. (1980). Many nonlinear systems exhibit approximately linear behavior when the input signal consists of small variations about a fixed operating point. These same systems may show gross nonlinearities when the input contains large disturbances that change the operating point of the system. The response of simple cells to the reverse correlation stimulus is more reminiscent of the former (small-signal) case, whereas the response to a single flash of a grating is more reminiscent of the latter case. Thus the differences between our findings and those of Tolhurst et al. (1980) may be related, at least partially, to the conditions of stimulation.

Another methodological issue involves the use of both luminance increments *and* decrements in characterizing the temporal response of simple cells. In the paradigm of Tolhurst et al. (1980), a stationary grating is flashed on at a single position within the receptive field. Thus, at a given receptive-field position, there is either a luminance increment *or* a luminance decrement. Because simple cells have little spontaneous discharge, inhibitory phases in the temporal (impulse) response cannot be observed. Failure to detect these inhibitory phases would lead to erroneous predictions of the temporal frequency tuning curve. In the reverse correlation method, each spatial position is tested with luminance increments *and* luminance decrements. By taking the difference between the responses to increments (bright bars) and decrements (dark bars) (see Figs. 2 and 3 of the companion paper, DeAngelis et al. 1993), inhibitory phases in the spatiotemporal response profile can be approximated. In other words, the effects of a threshold nonlinearity can be minimized by combining the responses to bright and dark stimuli. The assumption in this subtraction procedure is that the inhibition produced by a bright bar at a particular location within the receptive field may be

equated with the excitation produced by a dark bar at the same location. See the discussion below, as well as Palmer et al. (1991), for more on this point. Use of both increments and decrements may help to explain why we observe a better match between measured and predicted temporal frequency tuning curves, as compared with Tolhurst et al. (1980).

It has often been proposed that simple cells serve to encode scenes by performing a linear filtering of the visual image (Geisler and Hamilton 1986; Kulikowski and Bishop 1981b; Robson 1975, 1983; Sakitt and Barlow 1982; Watson 1983, 1987). In these models, only the spatial filtering characteristics of simple cells are generally considered. However, for these models to perform correctly on a spatiotemporal sequence of images, simple cells must behave linearly over both space *and* time. Our finding that both spatial and temporal summation in simple cells are approximately linear allows such models to be extended to the general case of a time-varying image.

Sources of nonlinearity

We have shown that the spatial and temporal frequency tuning of many simple cells (see Figs. 2 and 3) can be predicted from their spatiotemporal receptive-field profiles. However, Figs. 6 and 7 show that linear predictions of spatial and temporal frequency tuning parameters are not quite accurate. In particular, large errors are observed for the low-frequency cutoffs (Figs. 6C and 7C). We now consider nonlinearities that may account for these observations. One obvious candidate is a response threshold (or half-wave rectifier), because it is well known that most simple cells exhibit little maintained discharge in the absence of a visual stimulus. Tadmor and Tolhurst (1989) report that linear predictions of the spatial frequency tuning curve obtained via Fourier analysis of the line-weighting function can be markedly improved by incorporating a response threshold.

Overall, the data of Figs. 6 and 7 are consistent with the hypothesis that a response threshold is the main source of deviation from linearity. To see this, consider a hypothetical tuning curve that is Gaussian shaped on a linear frequency axis (which is a good approximation for spatial frequency tuning curves). Assume that the optimal frequency is 0.4 cycles/deg, the high cutoff frequency is 0.7 cycles/deg, and the low cutoff frequency is 0.1 cycles/deg. If we compute a predicted tuning curve via Fourier transform of a receptive-field profile, the effect of a response threshold will be to make the predicted tuning curve too broad (e.g., see Fig. 2 of Tadmor and Tolhurst 1989). Assume that the predicted tuning curve is broadened symmetrically such that it has a high cutoff frequency of 0.75 cycles/deg and a low cutoff frequency of 0.05 cycles/deg. The difference between the measured and predicted cutoff frequencies is 0.05 cycles/deg. For the high cutoff, this difference represents ~7% of the measured value; for the low cutoff, this difference amounts to 50% of the measured value. Thus the error in the low-frequency cutoff should be visible in our measurements, whereas the error in the high-frequency cutoff may be obscured by variability in the data.

The spatial frequency tuning data summarized in Fig. 7

are reasonably consistent with the effects of a response threshold. Predicted values of SF_{high} are, on average, 0.05 cycles/deg larger than measured values, and predicted values of SF_{low} are, on average, 0.08 cycles/deg smaller than measured values. The error at high frequencies is barely noticeable in Fig. 7B (because it represents a small fraction of the actual cutoff values), whereas the error at low frequencies is quite obvious in Fig. 7C. Although temporal frequency tuning curves are typically not Gaussian shaped on a linear frequency axis, a similar argument can be made concerning the effects of a response threshold on linear predictions. The data of Fig. 6 may also be consistent with the effects of a response threshold. Predicted values of TF_{high} are, on average, 0.25 Hz larger than measured values, and predicted values of TF_{low} are, on average, 0.32 Hz smaller than measured values. Again, the error is not very noticeable at high temporal frequencies (Fig. 6B) but is prominent at low temporal frequencies (Fig. 6C).

Although the data for our population of cells may be consistent with the effects of a threshold nonlinearity, some of the data from individual neurons are not consistent with this hypothesis. Some cells exhibit large deviations from linearity only at low spatial frequencies (Fig. 4A) or low temporal frequencies (Fig. 4B). These results are not consistent with the effects of a threshold because a threshold would effect both the low-and high-frequency ends of the curve. The combination of a threshold and an expansive nonlinearity (e.g., Albrecht and Geisler 1991; Heeger 1991, 1992b) also cannot account for these data, because the expansive nonlinearity would also act to broaden predicted tuning curves at both ends (see Heeger 1992b). One possible explanation for the data of Fig. 4, A and B, is that deviations from linearity at high spatial and temporal frequencies are masked by the blurring effect of finite dimension stimuli. If the bar stimuli used in the reverse correlation algorithm are too large (in space or time), high-frequency components in the data will be attenuated (see the companion paper for more on this point). Thus it is possible that the measured and predicted high cutoff frequencies match just by coincidence for some cells. However, this possibility can be discounted because we have corrected the data of Figs. 6 and 7 for any blurring effects of the stimulus, which are usually very small (see APPENDIX of the companion paper, DeAngelis et al. 1993).

Another possibility is that deviations at low spatial and temporal frequencies arise through frequency-specific intracortical inhibition. It has been reported (Bauman and Bonds 1991; DeValois and Tootell 1983) that the responses of many simple and complex cells to a grating of optimal spatial frequency can be inhibited by the superposition of a second grating having a different spatial frequency. This mechanism may act to sharpen the spatial frequency selectivity of some neurons (Bauman and Bonds 1991). However, it does not appear that this mechanism operates only at low frequencies. DeValois and Tootell (1983) report that spatial frequency-specific inhibition is only effective at high spatial frequencies for most cells. Bauman and Bonds (1991) report finding inhibition at both the low- and high-frequency ends of the tuning curve, with equal probability. Therefore it does not appear that this mechanism can ac-

count for deviations from linearity that are limited to low spatial frequencies.

Dean et al. (1982) have reported nonlinear interactions between two grating stimuli of different temporal frequencies. They report that the response of cells to a high temporal frequency stimulus is enhanced by the presence of a low temporal frequency stimulus, and that the response to a low-frequency stimulus is suppressed by the presence of a high-frequency stimulus. Recently, Reid et al. (1992) have confirmed and extended this finding with the use of a stimulus consisting of the sum of eight sinusoids of different temporal frequencies. It is possible that this type of nonlinearity accounts for some of the deviations from linearity that we have observed.

Another potential explanation for error in our linear predictions is that there are components of the receptive field that are not observable with the use of the techniques we have employed. Because simple cells do not produce any maintained discharge in the absence of a visual stimulus, we can only measure the excitatory inputs to a given neuron. The inhibitory inputs cannot be measured directly, without artificially raising the maintained discharge of the neuron. In constructing spatiotemporal receptive-field profiles with the use of the reverse correlation technique, we approximate the inhibitory inputs to a cell by taking the difference between responses to bright and dark stimuli. This procedure has also been used by several other researchers (e.g., Field and Tolhurst 1986; Jones and Palmer 1987a; Movshon et al. 1978; Palmer et al. 1991; Tadmor and Tolhurst 1989). The basic assumption is that inhibition produced by a bright stimulus is equivalent to excitation produced by a dark stimulus, and vice versa. As pointed out by Tadmor and Tolhurst (1989) and Palmer et al. (1991), failure of this assumption may account for errors in linear predictions of the responses to gratings. By allowing the inhibitory inputs to a neuron to differ in strength or spatial localization from the excitatory inputs, Palmer et al. (1991) have constructed a model that predicts the types of deviations from linearity that we have observed at low spatial frequencies. Further study will be necessary to determine whether explicit measurement of the inhibitory inputs to a neuron can improve predictions of spatial and temporal frequency selectivity.

Before leaving this topic, it should be pointed out that there are other types of nonlinearities known to modulate the response properties of simple cells (and complex cells). Most of these are probably generated within the local cortical neuronal network and can be considered dynamic nonlinearities, because their effect may depend on the recent history of the pattern of visual stimulation. One such nonlinearity is contrast gain control (Bonds 1991; Ohzawa et al. 1985; Sclar et al. 1989), which adjusts the dynamic range of a neuron on the basis of the recent history of contrast levels in the visual scene. Bonds (1991) has recently demonstrated that a contrast gain control mechanism may act rapidly when a cortical cell is stimulated by changes in contrast. Another well known nonlinearity is "cross-orientation" inhibition (Bonds 1989; DeAngelis et al. 1992; Morrone et al. 1982), by which the responses of two stimuli of different orientations interact nonlinearly for most cells. It is also known that many simple cells exhibit nonlineari-

ties of summation when tested with stimuli of different lengths (end-inhibition: e.g., Hubel and Wiesel 1965; Orban et al. 1979a,b) or widths (side-inhibition: Born and Tootell 1991; DeAngelis et al. 1990, 1991b; DeValois et al. 1985). Whether or not these various nonlinear interactions reflect different mechanisms is not yet clear. However, a recent model (Heeger 1992a) suggests that at least some of these effects may be explained by a single contrast normalization scheme, for which there is some physiological support (Bonds 1989, 1991; DeAngelis et al. 1992).

Direction selectivity

One of the prominent features of visual cortical cells is their direction selectivity for moving stimuli (see Orban 1991 for review). Despite many studies of direction selectivity in cortical neurons, there is no consensus in the literature concerning the mechanisms that underlie direction selectivity. Hubel and Wiesel (1959, 1962) reported that the responses of simple cells to moving stimuli could be predicted, qualitatively, from a mapping of the ON and OFF subregions of the receptive field. They suggested that a preference for a light bar moving in one direction might arise through summation of synchronized ON and OFF responses as the bar leaves an OFF subregion and enters an ON subregion. Several investigators (Bishop et al. 1974; Heggelund 1984; Henry and Bishop 1972; Peterhans et al. 1985; Yamane et al. 1985) have made predictions of direction selectivity from the arrangement of ON and OFF subregions in the spatial receptive-field profile (or line-weighting function) of simple cells. The consensus is that direction selectivity *cannot* be predicted from the spatial receptive-field profile. This result is not surprising, in retrospect, because the spatiotemporal receptive fields of direction-selective simple cells are not space-time separable. Hence, for these cells, there is no unique spatial receptive-field profile (see the companion paper for more on this point).

Failure to predict direction selectivity from the spatial receptive-field profile has led some researchers (cf. Heggelund 1984) to the conclusion that direction selectivity is mediated by (nonlinear) inhibitory interactions. Indeed, several models for the generation of direction selectivity in visual neurons (i.e., Barlow and Levick 1965; Bishop et al. 1971; Ruff et al. 1987; Schiller et al. 1976) have been formulated that rely on nonlinear (mostly inhibitory) interactions to explain the observed responses of cortical cells. Alternatively, theoretical studies (Adelson and Bergen 1985; Watson and Ahumada 1983, 1985) have suggested that the direction selectivity of simple cells in the visual cortex might derive from their linear spatiotemporal receptive-field structure. In particular, cells with *X-T* profiles that are inseparable, or tilted in space-time, are expected to exhibit a directional preference. Reid et al. (1987, 1991) have shown that linear predictions are accurate for determining the preferred direction for most simple cells. However, they report that the strength of the directional selectivity is typically underestimated by about a factor of two with the use of linear predictions. Similar findings have been reported by Albrecht and Geisler (1991) and Tolhurst and Dean (1991). In each of these studies, linear predictions are computed from the responses to counterphase modulated grat-

ings. We have obtained linear predictions of direction selectivity from measurements of the spatiotemporal receptive-field profile, and our findings are quite similar to those of Albrecht and Geisler (1991) and Reid et al. (1987, 1991). Our findings (Figs. 9 and 10) also complement those of McLean and Palmer (1989), who report that the optimal velocity of simple cells in response to a moving bar stimulus can be predicted from the spatiotemporal receptive-field profile measured with the use of reverse correlation.

The fact that linear predictions underestimate the measured direction selectivity index by a factor of two, on average (see Fig. 9D), suggests that nonlinear mechanisms are involved in generating direction selectivity. Recently, Albrecht and Geisler (1991) have shown that measured and predicted DSIs agree well when one compensates for the expansive exponential nonlinearity evident in the contrast-response function. We have confirmed the findings of Albrecht and Geisler (1991) for a subset of the simple cells recorded in this study. This result suggests that the linear spatiotemporal receptive field of simple cells is the basis for direction selectivity, and that direction selectivity is enhanced by a static exponential nonlinearity (Albrecht and Geisler 1991; see also a similar proposal by Heeger 1991, 1992b). If so, then the combination of a linear spatiotemporal filter and a static nonlinearity may account for both the direction selectivity and the temporal response properties (Mancini et al. 1990) of simple cells.

Although the exponent model (Albrecht and Geisler 1991; Heeger 1991, 1992b) accounts for the discrepancy between measured DSIs and linear predictions, it should be noted that this may not be a complete explanation of direction selectivity for simple cells. Both Reid et al. (1991) and Tolhurst and Dean (1991) report that linear predictions of a cell's response in the preferred direction are accurate, but predictions of the response in the nonpreferred direction are consistently too large. The exponent model (Albrecht and Geisler 1991) is consistent with the latter result but requires that linear predictions of the response in the preferred direction are *too small*. Hence it is possible that other mechanisms are involved. Reid et al. (1991) and Tolhurst and Dean (1991) both suggest that suppression of the response in the nonpreferred direction may account for the difference between measured and predicted DSIs. Recently, Heeger (1992c) has demonstrated that the combination of a static (exponent) nonlinearity and a contrast gain control mechanism may explain the observations of Reid et al. (1991) and Tolhurst and Dean (1991) concerning linear predictions of the responses in the preferred and nonpreferred directions.

With the use of a white noise method, Emerson and Citron (1989) and Emerson (1992) have shown that some simple cells exhibit nonlinear direction-selective subunits, which are similar to those found in complex cells (Emerson et al. 1987). These results may not be explained by a model consisting of a linear filter and a static nonlinearity (exponent). Jacobson et al. (1992) have also found, with the use of a white noise method, that the input-output relationships of simple cells in the monkey's striate cortex cannot be explained completely with the use of a model consisting of a linear filter followed by a static nonlinearity. Further research is necessary to elucidate which types of nonlineari-

ties may be involved in generating direction selectivity, so that a better model of simple-cell behavior may be formulated.

In summary, we have shown that spatiotemporal receptive-field profiles may be used to predict the spatial and temporal frequency selectivity of simple cells with reasonable accuracy (except at low frequencies in some cases). Consequently, reverse correlation measurements yield a reasonable approximation to the spatiotemporal impulse response for most simple cells. Accounting for some basic response nonlinearities, such as a response threshold and an expansive exponent, may improve the accuracy of some predictions, such as predictions of direction selectivity. Although several types of nonlinearities are known to modulate the responses of simple cells, these do not severely impair the usefulness of measurements of the spatiotemporal receptive-field profile.

APPENDIX

For a linear spatiotemporal filter, response increases proportionally with contrast (i.e., the contrast-response function is a straight line in linear coordinates). For a cortical neuron, however, the contrast-response function is nonlinear (see Fig. 10A). For low contrasts, response generally increases exponentially with contrast; for high contrasts, response saturates. Recently, simple cells have been modeled as a linear spatiotemporal filter combined with an expansive (exponential) nonlinearity and a contrast normalization mechanism (Albrecht and Geisler 1991; Heeger 1991, 1992a,b). The expansive nonlinearity accounts for the exponential increase in response for low contrasts. The contrast normalization mechanism accounts for the saturation of response at high contrasts. (We shall ignore the effect of a response threshold in the present discussion.) When the contrast of a visual stimulus is fixed (over some region of space and time), the contrast normalization factor becomes a constant. When one computes the ratio of two responses, this contrast normalization factor cancels out (see Albrecht and Geisler 1991 for additional details). Thus, to correct our estimates of DSIs (as in Fig. 10B), we need only consider the effect of the expansive nonlinearity (exponent).

We first consider the effect of the exponent on the DSI measured with the use of gratings. Let us denote the responses of a simple cell to a sinusoidal grating drifting in the preferred and opposite directions as R_p and R_{np} , respectively. These responses can be written as

$$R_p = (L_p)^n \quad \text{and} \quad R_{np} = (L_{np})^n$$

where L_p and L_{np} denote the output of the underlying linear filter to gratings drifting in the preferred and nonpreferred directions, respectively, and n is the exponent. We have computed a neuron's DSI, in response to gratings, by the formula

$$\text{DSI} = \frac{R_p - R_{np}}{R_p + R_{np}} = \frac{1 - \frac{R_{np}}{R_p}}{1 + \frac{R_{np}}{R_p}}$$

A DSI that is corrected for the effect of the exponent, n , can be written as

$$\text{DSI}_{\text{corr}} = \frac{1 - \frac{L_{np}}{L_p}}{1 + \frac{L_{np}}{L_p}} = \frac{1 - \left(\frac{R_{np}}{R_p}\right)^{\frac{1}{n}}}{1 + \left(\frac{R_{np}}{R_p}\right)^{\frac{1}{n}}}$$

where n is measured by fitting Eq. 4 to the contrast response function of the neuron (see Fig. 10A).

The procedure described above allows us to correct the DSI measured in response to grating stimuli. It is also necessary to correct the predicted DSI obtained via Fourier transform of the X - T profile (see Fig. 9, *B* and *C*). As described in the companion paper, the spatiotemporal receptive-field profile, $R(X, T)$, is obtained by taking the difference between responses to bright bars, $B(X, T)$, and responses to dark bars, $D(X, T)$

$$R(X, T) = B(X, T) - D(X, T)$$

An X - T profile that is corrected for the effect of the exponent, n , is computed as follows

$$R_{\text{corr}}(X, T) = B(X, T)^{1/n} - D(X, T)^{1/n}$$

$R_{\text{corr}}(X, T)$ is then Fourier transformed to obtain a spatiotemporal amplitude spectrum. A predicted DSI is then obtained as shown in Fig. 9C.

Corrected estimates of the measured and predicted DSI are shown for eight simple cells in Fig. 10B (●).

We are grateful to G. Ghose for participating in these experiments and for many helpful comments.

This work was supported by research and CORE grants from the National Eye Institute (EY-01175 and EY-03176) and by a collaborative project of the Human Frontier Science Program.

Address for reprint requests: R. D. Freeman, School of Optometry, 360 Minor Hall, University of California, Berkeley, Berkeley, CA 94720.

Received 3 August 1992; accepted in final form 16 November 1992.

REFERENCES

- ADELSON, E. H. AND BERGEN, J. R. Spatio-temporal energy models for the perception of motion. *J. Opt. Soc. Am. A* 2: 284–299, 1985.
- ALBRECHT, D. G., DEVALOIS, R. L., AND THORELL, L. G. Visual cortical neurons: are bars or gratings the optimal stimuli? *Science Wash. DC* 207: 88–90, 1980.
- ALBRECHT, D. G. AND GEISLER, W. S. Motion selectivity and the contrast-response function of simple cells in the visual cortex. *Visual Neurosci.* 7: 531–546, 1991.
- ALBRECHT, D. G. AND HAMILTON, D. B. Striate cortex of monkey and cat: contrast response function. *J. Neurophysiol.* 48: 217–237, 1982.
- ANDREWS, B. W. AND POLLEN, D. A. Relationship between spatial-frequency selectivity and receptive-field profile of simple cells. *J. Physiol. Lond.* 287: 163–176, 1979.
- BAKER, C. L. AND CYNADER, M. S. Spatial receptive-field properties of direction-selective neurons in cat striate cortex. *J. Neurophysiol.* 55: 1136–1152, 1986.
- BARLOW, H. B. AND LEVICK, W. R. The mechanism of directionally selective units in rabbit's retina. *J. Physiol. Lond.* 178: 477–506, 1965.
- BAUMAN, L. A. AND BONDS, A. B. Inhibitory refinement of spatial frequency selectivity in single cells of the cat striate cortex. *Vision Res.* 31: 933–944, 1991.
- BISHOP, P. O., COOMBS, J. S., AND HENRY, G. H. Responses to visual contours: spatiotemporal aspects of excitation in the receptive fields of simple striate neurones. *J. Physiol. Lond.* 219: 625–657, 1971.
- BISHOP, P. O., GOODWIN, A. W., AND HENRY, G. H. Direction selective sub-regions in striate simple cell receptive fields (Abstract). *J. Physiol. Lond.* 238: 25P–27P, 1974.
- BONDS, A. B. Role of inhibition in the specification of orientation selectivity of cells in the cat striate cortex. *Visual Neurosci.* 2: 41–55, 1989.
- BONDS, A. B. Temporal dynamics of contrast gain in single cells of the cat striate cortex. *Visual Neurosci.* 6: 239–255, 1991.
- BORN, R. T. AND TOOTELL, R. B. H. Single-unit and 2-deoxyglucose studies of side inhibition in macaque striate cortex. *Proc. Natl. Acad. Sci. USA* 88: 7071–7075, 1991.
- CAMPBELL, F. W., COOPER, G. F., AND ENROTH-CUGELL, C. The spatial selectivity of the visual cells of the cat. *J. Physiol. Lond.* 203: 223–235, 1969.
- COOPER, G. F. AND ROBSON, J. G. Successive transformations of spatial information in the visual system. *IEE Natl. Physiol. Lab. Conf. Proc.* 42: 134–143, 1968.
- DAUGMAN, J. G. Uncertainty relation for resolution in space, spatial frequency, and orientation optimized by two-dimensional visual cortical filter. *J. Opt. Soc. Am. A* 2: 1160–1169, 1985.
- DEAN, A. F., TOLHURST, D. J., AND WALKER, N. S. Non-linear temporal summation by simple cells in cat striate cortex demonstrated by failure of superposition. *Exp. Brain Res.* 45: 456–458, 1982.
- DEANGELIS, G. C., OHZAWA, I., AND FREEMAN, R. D. Depth is encoded in the visual cortex by a specialized receptive field structure. *Nature Lond.* 352: 156–159, 1991a.
- DEANGELIS, G. C., OHZAWA, I., AND FREEMAN, R. D. Spatiotemporal organization of simple-cell receptive fields in the cat's striate cortex. I. General characteristics and postnatal development. *J. Neurophysiol.* 69: 1091–1117, 1993.
- DEANGELIS, G. C., OHZAWA, I., FREEMAN, R. D., AND GHOSE, G. M. Properties of length and width tuning of cells in the cat's striate cortex (Abstract). *Invest. Ophthalmol. Visual Sci. Suppl.* 31: 430, 1990.
- DEANGELIS, G. C., ROBSON, J. G., OHZAWA, I., AND FREEMAN, R. D. Spatial organization of inhibitory influences upon neurons in the cat's striate cortex. *Soc. Neurosci. Abstr.* 17: 1016, 1991b.
- DEANGELIS, G. C., ROBSON, J. G., OHZAWA, I., AND FREEMAN, R. D. Organization of suppression in receptive fields of neurons in cat visual cortex. *J. Neurophysiol.* 68: 144–163, 1992.
- DEVALOIS, K. K., DEVALOIS, R. L., AND YUND, E. W. Responses of striate cortical cells to grating and checkerboard patterns. *J. Physiol. Lond.* 291: 483–505, 1979.
- DEVALOIS, K. K. AND TOOTELL, R. B. H. Spatial-frequency-specific inhibition in cat striate cortex cells. *J. Physiol. Lond.* 336: 359–376, 1983.
- DEVALOIS, R. L., ALBRECHT, D. G., AND THORELL, L. G. Cortical cells: bar and edge detectors or spatial-frequency analyzers? In: *Frontiers in Visual Science*, edited by S. J. Cool and E. L. Smith. New York: Springer-Verlag, 1978, p. 544–556.
- DEVALOIS, R. L., ALBRECHT, D. G., AND THORELL, L. G. Spatial frequency selectivity of cells in macaque visual cortex. *Vision Res.* 22: 545–559, 1982.
- DEVALOIS, R. L., THORELL, L. G., AND ALBRECHT, D. G. Periodicity of striate cortex cell receptive fields. *J. Opt. Soc. Am. A* 2: 1115–1122, 1985.
- EMERSON, R. C. Do directionally selective simple cells use motion-energy subunits (Abstract)? *Invest. Ophthalmol. Visual Sci. Suppl.* 33: 953, 1992.
- EMERSON, R. C. AND CITRON, M. C. Linear and nonlinear mechanisms of motion selectivity in single neurons of the cat's visual cortex. In: *Proceedings IEEE Conference on Systems, Man, and Cybernetics*, edited by D. L. Kleinman. Cambridge, MA: IEEE, 1989, p. 448–453.
- EMERSON, R. C., CITRON, M. C., VAUGHN, W. J., AND KLEIN, S. A. Non-linear directionally selective subunits in complex cells of cat striate cortex. *J. Neurophysiol.* 58: 33–65, 1987.
- FIELD, D. J. AND TOLHURST, D. J. The structure and symmetry of simple-cell receptive-field profiles in the cat's visual cortex. *Proc. R. Soc. Lond. B Biol. Sci.* 228: 379–400, 1986.
- GABOR, D. Theory of communication. *J. Inst. Electr. Eng.* 93: 429–457, 1946.
- GEISLER, W. S. AND HAMILTON, D. B. Sampling-theory analysis of spatial vision. *J. Opt. Soc. Am. A* 3: 62–70, 1986.
- GLEZER, V. D., TSCHERBACH, T. A., GAUSELMAN, V. E., AND BONDARKO, V. M. Linear and nonlinear properties of simple and complex receptive fields in area 17 of the cat visual cortex. *Biol. Cybern.* 37: 195–208, 1980.
- GLEZER, V. D., TSCHERBACH, T. A., GAUSELMAN, V. E., AND BONDARKO, V. M. Spatio-temporal organization of receptive fields of the cat's striate cortex. *Biol. Cybern.* 43: 35–49, 1982.
- HEEGER, D. J. Non-linear model of neural responses in cat visual cortex. In: *Computational Models of Visual Processing*, edited by M. S. Landy, and J. A. Movshon. Cambridge, MA: MIT Press, 1991, p. 119–133.
- HEEGER, D. J. Normalization of cell responses in cat striate cortex. *Visual Neurosci.* 9: 181–197, 1992a.
- HEEGER, D. J. Half-squaring in responses of cat striate cells. *Visual Neurosci.* 9: 427–443, 1992b.
- HEEGER, D. J. Modelling simple cell direction selectivity with normalized, half-squared, linear operators (Abstract). *Invest. Ophthalmol. Visual Sci. Suppl.* 33: 953, 1992c.
- HEGGELUND, P. Direction asymmetry by moving stimuli and static receptive field plots for simple cells in cat striate cortex. *Vision Res.* 24: 13–16, 1984.
- HENRY, G. H. AND BISHOP, P. O. Striate neurons: receptive field organization. *Invest. Ophthalmol.* 11: 357–368, 1972.

- HUBEL, D. H. AND WIESEL, T. N. Receptive fields of single neurones in the cat's striate cortex. *J. Physiol. Lond.* 148: 574–591, 1959.
- HUBEL, D. H. AND WIESEL, T. N. Receptive fields, binocular interaction and functional architecture in the cat's visual cortex. *J. Physiol. Lond.* 160: 106–154, 1962.
- HUBEL, D. H. AND WIESEL, T. N. Receptive fields and functional architecture in two non-striate visual areas (18 and 19) of the cat. *J. Neurophysiol.* 41: 229–289, 1965.
- JACOBSON, L. D., GASKA, J. P., CHEN, H.-W., AND POLLON, D. A. Quantitative testing of multi-input LN and LNL models for monkey V1 cells (Abstract). *Invest. Ophthalmol. Visual Sci. Suppl.* 33: 1022, 1992.
- JONES, J. P. AND PALMER, L. A. The two-dimensional spatial structure of simple receptive fields in the cat striate cortex. *J. Neurophysiol.* 58: 1187–1211, 1987a.
- JONES, J. P. AND PALMER, L. A. An evaluation of the two-dimensional Gabor filter model of simple receptive fields in cat striate cortex. *J. Neurophysiol.* 58: 1233–1258, 1987b.
- KULIKOWSKI, J. J. AND BISHOP, P. O. Linear analysis of the responses of simple cells in the cat visual cortex. *Exp. Brain Res.* 44: 386–400, 1981a.
- KULIKOWSKI, J. J. AND BISHOP, P. O. Fourier analysis and spatial representation in the visual cortex. *Experientia Basel* 37: 161–163, 1981b.
- LINDSAY, P. M. AND NORMAN, D. A. *Human Information Processing*. New York: Academic, 1972.
- MAFFEI, L. AND FIORENTINI, A. The visual cortex as a spatial frequency analyzer. *Vision Res.* 13: 1255–1267, 1973.
- MAFFEI, L., MORRONE, C., PIRCHIO, M., AND SANDINI, G. Responses of visual cortical cells to periodic and nonperiodic stimuli. *J. Physiol. Lond.* 296: 27–47, 1979.
- MANCINI, M., MADDEN, B. C., AND EMERSON, R. C. White noise analysis of temporal properties in simple receptive fields of cat cortex. *Biol. Cybern.* 63: 209–219, 1990.
- MARCELJA, S. Mathematical description of the responses of simple cortical cells. *J. Opt. Soc. Am.* 70: 1297–1300, 1980.
- MCLEAN, J. AND PALMER, L. A. Contribution of linear spatiotemporal receptive field structure to velocity selectivity of simple cells in the cat's striate cortex. *Vision Res.* 29: 675–679, 1989.
- MORRONE, M. C., BURR, D. C., AND MAFFEI, L. Functional implications of cross-orientation inhibition of cortical visual cells. *Proc. R. Soc. Lond. B Biol. Sci.* 216: 335–354, 1982.
- MOVSHON, J. A., THOMPSON, I. D., AND TOLHURST, D. J. Spatial summation in the receptive fields of simple cells in the cat's striate cortex. *J. Physiol. Lond.* 283: 53–77, 1978.
- OHZAWA, I., SCLAR, G., AND FREEMAN, R. D. Contrast gain control in the cat's visual system. *J. Neurophysiol.* 54: 651–667, 1985.
- ORBAN, G. A., KATO, H., AND BISHOP, P. O. End-zone region in receptive fields of hypercomplex and other striate neurons in the cat. *J. Neurophysiol.* 42: 818–832, 1979a.
- ORBAN, G. A., KATO, H., AND BISHOP, P. O. Dimensions and properties of end-zone inhibitory areas in receptive fields of hypercomplex cells in cat striate cortex. *J. Neurophysiol.* 42: 833–849, 1979b.
- ORBAN, G. A. Quantitative electrophysiology of visual cortical neurones. In: *Vision and Visual Dysfunction. The Neural Basis of Visual Function*, edited by A. G. Leventhal. Boca Raton, FL: CRC, 1991, vol. 4, p. 173–222.
- PALMER, L. A., JONES, J. P., AND STEPNOISKI, R. A. Striate receptive fields as linear filters: characterization in two dimensions of space. In: *Vision and Visual Dysfunction. The Neural Basis of Visual Function*, edited by A. G. Leventhal. Boca Raton, FL: CRC, 1991, vol. 4, p. 246–265.
- PETERHANS, E., BISHOP, P. O., AND CAMARDA, R. M. Direction selectivity of simple cells in cat striate cortex to moving light bars. I. Relation to stationary flashing bar and moving edge responses. *Exp. Brain Res.* 57: 512–522, 1985.
- PRESS, W. H., FLANNERY, B. P., TEUKOLSKY, S. A., AND VETTERLING, W. T. *Numerical Recipes in C*. New York: Cambridge Univ. Press, 1988.
- REID, R. C., SOODAK, R. E., AND SHAPLEY, R. M. Linear mechanisms of directional selectivity in simple cells of cat striate cortex. *Proc. Natl. Acad. Sci. USA* 84: 8740–8744, 1987.
- REID, R. C., SOODAK, R. E., AND SHAPLEY, R. M. Directional selectivity and spatiotemporal structure of receptive fields of simple cells in cat striate cortex. *J. Neurophysiol.* 66: 505–529, 1991.
- REID, R. C., VICTOR, J. D., AND SHAPLEY, R. M. Broadband temporal stimuli decrease the integration time of neurons in cat striate cortex. *Visual Neurosci.* 9: 39–45, 1992.
- ROBSON, J. G. Receptive fields: neural representation of the spatial and intensive attributes of the visual image. In: *Handbook of Perception*, edited by E. C. Carterette and M. P. Friedman. New York: Academic, 1975, vol. 5, p. 81–116.
- ROBSON, J. G. Frequency domain visual processing. In: *Physical and Biological Processing of Images*, edited by O. J. Braddick and A. C. Sleigh. Berlin: Springer-Verlag, 1983, p. 73–87.
- RUFF, P. I., RAUSCHECKER, J. P., AND PALM, G. A model of direction-selective "simple" cells in the visual cortex based on inhibition asymmetry. *Biol. Cybern.* 57: 147–157, 1987.
- SAKITT, B. AND BARLOW, H. B. A model for the economical encoding of the visual image in cerebral cortex. *Biol. Cybern.* 43: 97–108, 1982.
- SCHILLER, P. H., FINLAY, B. L., AND VOLMAN, S. F. Quantitative studies of single cell properties in monkey striate cortex. I. Spatiotemporal organization of receptive fields. *J. Neurophysiol.* 39: 1288–1319, 1976.
- SCLAR, G., LENNIE, P., AND DEPRIEST, D. D. Contrast adaptation in striate cortex of macaque. *Vision Res.* 29: 747–755, 1989.
- TADMOR, Y. AND TOLHURST, D. J. The effect of threshold on the relationship between the receptive-field profile and the spatial frequency tuning curve in simple cells of the cat's striate cortex. *Visual Neurosci.* 3: 445–454, 1989.
- TOLHURST, D. J. AND DEAN, A. F. Evaluation of a linear model of directional selectivity in simple cells of the cat's striate cortex. *Visual Neurosci.* 6: 421–428, 1991.
- TOLHURST, D. J., WALKER, N. S., THOMPSON, I. D., AND DEAN, A. F. Non-linearities of temporal summation in neurones in area 17 of the cat. *Exp. Brain Res.* 38: 431–435, 1980.
- WATSON, A. B. Detection and recognition of simple spatial forms. In: *Physical and Biological Processing of Images*, edited by O. J. Braddick and A. C. Sleigh. Berlin: Springer-Verlag, 1983, p. 100–114.
- WATSON, A. B. Efficiency of a model human image code. *J. Opt. Soc. Am. A* 4: 2401–2417, 1987.
- WATSON, A. B. AND AHUMADA, A. J. A look at motion in the frequency domain. *NASA Tech. Memo.* 84352: 1–10, 1983.
- WATSON, A. B. AND AHUMADA, A. J. Models of human visual-motion sensing. *J. Opt. Soc. Am. A* 2: 322–342, 1985.
- WEBSTER, M. A. AND DEVALOIS, R. L. Relationship between spatial-frequency and orientation tuning of striate-cortex cells. *J. Opt. Soc. Am. B* 2: 1124–1132, 1985.
- YAMANE, S., MASKE, R., AND BISHOP, P. O. Direction selectivity of simple cells in cat striate cortex to moving light bars. II. Relation to moving dark bar responses. *Exp. Brain Res.* 57: 523–536, 1985.